# PERFORMANCE EVALUATION OF A LOW-COST SENSOR FOR CONTINUOUS METHANE MONITORING

by

Colleen Gosse

Submitted in partial fulfilment of the requirements
for the degree of Master of Applied Science

at

Dalhousie University
Halifax, Nova Scotia
June 2022

© Copyright by Colleen Gosse, 2022

DEDICATION PAGE

Dedicated to Kevin Chisholm (1940-2022) whose thoughtful questions about the results of this work will be greatly missed along with his brilliantly engineered solutions

# TABLE OF CONTENTS

## LIST OF TABLES

## LIST OF FIGURES

## ABSTRACT

Methane is a significant contributor to climate change. Methane emissions can be estimated by top-down methods or bottom-up methods and the methane budgets calculated by these two methods can vary by up to 50%. Understanding methane sources and sinks is critical to managing emissions and to mitigate climate change. The lack of observation systems capable of measuring the temporal variability of many sources over short and long timescales accounts for some of the disagreements in budgets. Current measurement methods are costly and inadequate for long term, continuous monitoring. Low-cost methane sensors, such as metal oxide semiconductor sensors, are needed for accurate methane budgets, but these sensors are sensitive to changes in temperature and humidity. A metal oxide semiconductor sensor was evaluated in a laboratory and based on the results of that testing an environmentally controlled enclosure was developed to control temperature and humidity. The sensor was installed inside of the environmentally controlled enclosure was tested in the laboratory, in a controlled field environment and at an active industrial site to assess the impact of controlling temperature and humidity on the sensor's accuracy. The field testing at an industrial site highlighted the expected emissions profile with short pulse events, which were difficult for the MOS sensor to accurately measure in short succession. The emissions profile of the source being measured should be considered in the future use of MOS sensors. The results of the testing demonstrated humidity had the strongest influence on sensor response. In a laboratory environment, the sensor measured methane concentrations with a root mean square error of 1.3 ppm. The enclosure stabilized temperature within 2.5°C and relative humidity within 4%. Use of the enclosure improved sensor accuracy but to calculate emissions estimates an error estimate under field conditions would need to be less than 1 ppm. The sensor was able to detect large emission events and would be suitable as a tool to alert the user to large changes in methane concentration, but additional refinements to the sensor to improve the error are required to use it in long term continuous monitoring applications. The sensor, as it was used in this research, would be best suited used in conjunction with more accurate measurement tools to support improvements to the methane budget. The MOS sensor can support improved methane management by alerting a user of a large release above baseline.

## LIST OF ABBREVIATIONS USED

| | |
|---|---|
| $CH_4$ | Methane |
| $CO_2$ | Carbon dioxide |
| LiDAR | Light detection and ranging system |
| MOS | Metal oxide semiconductor |
| NDIR | Non-dispersive infrared |
| PCB | Printed circuit board |
| ppb | Parts per billion |
| ppm | Parts per million |
| RMSE | Root mean square error |
| SD | Standard deviation |
| $SnO_2$ | Tin dioxide |
| SWIR | Shortwave infrared |

## ACKNOWLEDGEMENTS

This research and the project were challenging for me, and it would not have happened without a great deal of support for which I am so appreciative. Firstly, I am immensely grateful and indebted to my supervisors Dr. Manuel Helbig and Dr. Barret Kurylyk. Their guidance, expertise and patience has been invaluable, and this project would not have been possible without them. I would also like to thank Nick, Chance, Darren and Alex, along with everyone at Eosense for their support and for answering my many questions along the way. Thank you to my committee members, Dr. Rachel Chang and Dr. Rob Jamieson, for their time and their helpful feedback. Thank you to the Coastal Hydrology lab and the Land-Atmosphere Interaction lab colleagues for their help and advice. Thank you to Dr. Mark Gibson and the AFRG (especially Ellen, Loay and Codey) and thank you to the Civil and Resource Engineering Department staff. Thank you to NSERC for funding a portion of the project. Thank you to Christian for the encouragement every step of the way and for keeping me fed. Thank you to my parents and my sister for their support and for not asking “are you done yet?”. Thank you to my friends (especially Sam for helping me learn R) and extended family for continuing to invite me to get together, and I look forward to hopefully having more free time and seeing much more of you. Thank you to the women of my mentor POD who have kept me motivated through the challenges these past two years have brought.

# CHAPTER 1 INTRODUCTION

## 1.1 Global Methane Budget and Contributions to Climate Change

Methane ($CH_4$) is an important greenhouse gas and a major contributor to global climate change. $CH_4$ in the atmosphere accounts for nearly 17% of the radiative forcing of Earth's climate (Myhre et al., 2013), which is second only to carbon dioxide ($CO_2$). $CH_4$ has a higher Global Warming Potential than $CO_2$. Over 20 years, an equivalent emission of $CH_4$ would have 80 to 83 times the radiative forcing of $CO_2$ (Forster et al., 2021). However, $CH_4$ has a shorter atmospheric lifetime (12 years, Forster et al., 2021) than $CO_2$, which can reside in the atmosphere for thousands of years (Joos et al., 2013). It is estimated that 50-65% of $CH_4$ emissions originate from anthropogenic sources (Saunois et al., 2020). The shorter lifespan of $CH_4$ in the atmosphere and large anthropogenic contributions provide the impetus to mitigate its climate change impacts and thus have a more immediate effect on global temperature increases (Nisbet et al., 2020).

Identifying and quantifying key $CH_4$ sources and sinks remains a challenge leading to large uncertainties in current $CH_4$ budgets (Allen, 2016; Jackson et al., 2020; Kirschke et al., 2013; Lan et al., 2021; Myhre et al., 2013; Saunois et al., 2020). $CH_4$ sources and sinks are governed by complex biogeochemical cycles. There have been increases in anthropogenic emissions, and humans have also altered Earth's natural biogeochemical cycles (Ito & Inatomi, 2012). Sources of natural $CH_4$ include wetlands, fresh water, wild animals, wildfires, termites, geological formations, hydrates, and permafrost. Sources of anthropogenic $CH_4$ include agriculture, waste, biomass burning, and fossil fuels. In Canada, more than 50% of total anthropogenic greenhouse gas emissions can be attributed to combustion and fugitive sources from the energy industry (Environment and

Climate Change Canada, 2020). Sources of $CH_4$ in the oil and gas industry are poorly understood (Chan et al., 2020), and large sources, such as tank venting, have been underestimated (Lyon et al., 2016) due to their intermittent nature making them difficult to accurately measure with current observations systems. In general, natural $CH_4$ emissions inventories have an uncertainty of up to 50%, and anthropogenic sources have uncertainty up to 30% (Kirschke et al., 2013).

Global $CH_4$ budgets are largely calculated using a combination of top-down and bottom-up measurements as well as modeling. Top-down approaches use atmospheric observations and chemical transport models to estimate sources (National Academies of Sciences Engineering and Medicine, 2018). Satellite and aerial observations of atmospheric $CH_4$ concentrations are used in models or mass balances to estimate ground emission rates (Peischl et al., 2016; Thompson et al., 2015). The bottom-up methods use ground-based flux measurements or estimates, and extrapolations based on scaling factors for different emission types (National Academies of Sciences Engineering and Medicine, 2018), along with process-based land surface models (Saunois et al., 2020).

Inventories calculated using these different methods have resulted in poor agreement to date (National Academies of Sciences Engineering and Medicine, 2018) with wetland and fossil fuel source calculations having disagreements of 33% to 50% between top-down and bottom-up methods (Saunois et al., 2020). The large difference between observation-based estimates can be attributed to several reasons including a lack of surface flux measurements in space and time (Knox et al., 2019; Saunois et al., 2016). $CH_4$ emissions are highly variable over time, yet most measurements do not provide continuous, high-frequency time series of $CH_4$ emissions. Emission rates can vary up to

100% during a day (Vaughn et al., 2018). Emissions can also occur as short-term pulse events due to processes such as venting at an industrial site or ebullition in a wetland. To reduce uncertainties of top-down estimates, surface measurement constraints with high spatial and temporal coverage are required (Dlugokencky et al., 2011). The Committee on Anthropogenic Methane Emissions recommended a comprehensive grid with a resolution of at least 0.1° x 0.1° (approximately 100 $km^2$) to continuously monitor $CH_4$ emissions using concentration measurements and flux calculations (National Academies of Sciences Engineering and Medicine, 2018). Continuous monitoring has the potential to reduce the discrepancy between top-down and bottom-up inventories by capturing temporal variability (Vaughn et al., 2018).

### 1.2 Measurement Methods

Atmospheric $CH_4$ is present in the air at a mixing ratio of approximately 1.9 parts per million (ppm) as of October 2020 (Dlugokencky, 2020). The low concentration makes $CH_4$ more difficult to detect compared to the more abundant carbon dioxide, which has a concentration more than 200 times higher (Dlugokencky, 2020; Tans & Keeling, 2018). This makes $CH_4$ measurements challenging, and several tools are available to measure $CH_4$ concentrations and $CH_4$ fluxes. As mentioned previously, the approaches to quantify $CH_4$ budgets fall into two main categories: top down and bottom up.

Top-down methods employ satellites, aircraft, or drones equipped with sensors to measure absorption spectroscopy or infrared spectroscopy or a light detection and ranging system (LiDAR). Currently, four satellites with $CH_4$ measurement instrumentation (IASI, TROPOMI, CrIS and GOSAT2) are being used by government agencies to measure $CH_4$ (Brown et al., 2021). An additional five satellites are scheduled

to be launched in 2022 and 2023 (MERLIN, Sentinel-5, geoCARB, IASI-NG, IRS) (Brown et al., 2021; World Meteorological Institute, n.d.). There are also private companies and nonprofit organizations launching dedicated satellites for $CH_4$ monitoring, such as GHGSat and Bluefield Methane, MethaneSAT (Gallucci, 2020). The privately launched satellites often target areas with commercial interests such as areas with a high density of oil and gas activities, and report a much finer resolution than the publicly funded research satellites (Elkind et al., 2020). The satellites currently in operation use passive shortwave infrared (SWIR) and thermal infrared instruments to measure $CH_4$ as $CH_4$ absorbs radiation at 1.65 and 2.3 µm in shortwave infrared and 8 µm in thermal infrared. Table 1 shows a summary of current and future satellites used for the measurement of $CH_4$ concentrations.

Table 1: $CH_4$ monitoring satellites (existing and *planned*) (adapted from Ehret et al., 2017; Jacob et al., 2016).

| **Satellite** | **IASI** | **CrIS/ NOAA-20** | **TROPOMI/ Sentinel-5P** | **GOSAT-2** | ***MERLIN*** | ***Sentinel-5*** | ***geoCARB*** | ***IASI-NG*** | ***IRS*** |
|---|---|---|---|---|---|---|---|---|---|
| Detector | Thermal | Cross-track Infrared Sounder | Passive SWIR | Passive SWIR | *LIDAR* | *Passive SWIR* | *Passive SWIR* | *Thermal* | *Infra Red Sounder* |
| $CH_4$ spectral window (µm) | 3.62-15.50 | 1.63-1.70 | 2.31-2.39 | 1.63-1.70 2.33-2.38 | *1.64* | *1.63-1.70 2.31-2.39* | *2.3-2.34* | *3.62-15.56* | *4.3-7.7* |
| Launch year | 2007 | 2009 | 2017 | 2018 | *2022* | *2022* | *2022/23* | *2023* | *2023* |
| Spatial resolution ($km^2$) | 144 | 100 | 49 | 100 | *0.0225* | *49* | *20* | *144* | *64* |

Top-down methods provide a tool to monitor regional $CH_4$ emissions, but given their resolution on the scale of kilometers, they are not suitable for identifying point sources of emissions. In order to generate effective $CH_4$ mitigation policy, information such as

which sources are the largest contributors to national $CH_4$ emissions is critical. The spatial resolution as well as the typical minimum detected flux rates provided by top-down methods are not adequate, on their own, to support effective mitigation policies.

### 1.3 Methane Detectors

Historically, ground-based measurements of atmospheric $CH_4$ concentrations have relied on gas chromatography with a flame ionization detector (Dlugokencky et al., 1995; Saunois et al., 2016). More recently, spectroscopy, specifically cavity ring-down spectrometry, has been the preferred method for continuous $CH_4$ measurements (Zellweger et al., 2016). Both gas chromatography and spectroscopy instruments are highly accurate; however, they require grid power and are costly to purchase, and gas chromatography instruments require regular user input and carrier gases to run properly. As such, they are not well suited for a large-scale, distributed monitoring network or monitoring grid previously described. Other methods that have been used for the detection of atmospheric $CH_4$ include infrared sensors, catalytic bead sensors, electrochemical sensors, and metal oxide semiconductor sensors. Other more experimental methods, such as photoacoustic detectors, biosensors, calorimetric, and piezoelectric sensors (Lawrence, 2006), have also been used.

Infrared sensors are used extensively in handheld leak detecting instruments. Non-dispersive infrared (NDIR) sensors are low-power, low-cost and well-suited for continuous monitoring of gases present in high mixing ratios. Recent testing in a laboratory environment has shown the potential for ppm-level measurements of $CH_4$ concentrations (Zhu et al., 2012), but the lowest current detection limits for $CH_4$ are approximately 500 ppm. Infrared sensors are also prone to spectral interferences (Dinh et

al., 2016). Catalytic bead sensors measure a change in resistance as a result of flammable gases oxidizing on the surface of the sensing element. They represent a poisoning risk and are better suited to measuring high $CH_4$ concentrations. Recent studies using catalytic bead sensors were capable of observing $CH_4$ concentrations of 1,000 to 10,000 ppm (Liu et al., 2011).

Electrochemical sensors measure a change in current across a working electrode and a reference electrode when the presence of $CH_4$ causes an oxidation reaction on the working electrode. Some electrochemical sensors require the use of dangerous acidic fluids, and others require high temperatures to operate (Aldhafeeri et al., 2020). Sensors using photoacoustic spectroscopy have been demonstrated to have a detection limit down to 0.3 ppm (Besson et al., 2006; Rouxel et al., 2015), but they have high power requirements and are not currently commercially available on the market. Biosensors have detection limits of approximately 3,000 ppm in water (Wen et al., 2008) and are better suited for dissolved $CH_4$ measurements. Calorimetric-thermoelectric gas sensors have been shown to measure gas concentrations down to 1 ppm (Nagai et al., 2015), but have not been studied extensively. These sensors are also sensitive to drift in their response and to temperature and humidity variations. Piezoelectric sensors, which are sensitive to temperature and humidiy, have been studied to detect $CH_4$ concentrations as low as 500 ppm (Sun et al., 2009).

The $CH_4$ sensors described above are not suitable for deployment in a dense, distributed network to measure changes in atmospheric levels of $CH_4$. They have cost, power, and/or practical limitations, which would prevent their use in large scale monitoring networks (Table 2).

Table 2: Relative comparison of common $CH_4$ detectors.

| | Cost | Power | Selectivity | Sensitivity | Detection Limit |
|---|---|---|---|---|---|
| Gas Chromatography – Flame Ionization | High | High | High | High | Low |
| Cavity Ringdown Spectroscopy | High | High | High | High | Low |
| Infrared Sensors | Low-Medium | Low | Medium | Low | High |
| Electrochemical sensors | Low | Medium | Medium | Medium | Medium |
| Metal Oxide Semiconductor | Low | Low | Low-Medium | Medium | Medium-High |

Metal oxide semiconductor (MOS) sensors are another sensor type that can be used to measure atmospheric $CH_4$ concentrations. They are solid-state sensors with a demonstrated potential for use in a distributed, continuous monitoring network. These sensors are low power, lightweight, have fast response times and are inexpensive (Collier-Oxandale et al., 2018).

### 1.4 MOS Sensor Operating Principles

Metal Oxide Semiconductor (MOS) sensors consist of a metal oxide substrate on a heated element. When heated, oxygen atoms bond to the surface of the semiconductor by trapping free electrons. Tin dioxide ($SnO_2$) is a common MOS substrate for combustible hydrocarbons. When an $SnO_2$ semiconductor is exposed to a reducing gas, these oxygen atoms react with the gas and cause the resistance across the semiconductor to decrease as the electrons are free to flow again (Figure 1).

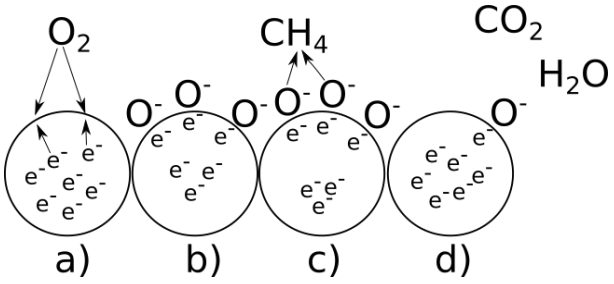


Figure 1 MOS Diagram (modified from Filipovic & Selberherr, 2015; Peterson et al., 2017; Wang et al., 2010): a) oxygen atoms bond to surface when heated, b) oxygen ions trap electrons when bonded to surface, c) sample gas reacts with oxygen atoms, and d) electrons are released and resistance decreases.

### 1.5 MOS Sensors for Atmospheric Monitoring

Metal oxide semiconductor sensors have several challenges that currently inhibit their use in a distributed monitoring network. MOS sensors have been shown to suffer from cross sensitivities to other oxidizable gases (poor selectivity), as well as from variable sensor responses depending on the metals used as semiconductors, the sensing mechanism (electron donors or receivers), and the semiconductor surface (Wang et al., 2010). Advances in sensor design have improved many of these factors, and more recent research highlights environmental sensitivities and sensor drift over time as two of the most important but inadequately addressed issues facing MOS sensors currently on the market (Bastviken et al., 2020; Collier-Oxandale et al., 2018; Eugster & Kling, 2012; Peterson et al., 2017; Van Den Bossche et al., 2017).

Sensor baseline drift is the gradual change in sensor response over time. For metal oxide sensors, this is typically the result of changes to the resistance of the heating element (Masson et al., 2015). As the resistance in the heating element decreases over time, the temperature increases. The effect of sensor drift has been reported to be in the range of

0.01 ppm per week (Eugster & Kling, 2012). Pearce et al. (2003) have demonstrated that the sensor response is strongly affected by changes to the sensor surface temperature.

Similarly, ambient environmental temperature and humidity have also been shown to have a strong effect on metal oxide sensors and influence the sensor response to a sample (Eugster & Kling, 2012; Wang et al., 2010). In comparison to sensor baseline drift where changes to the resistive heater happen over a long period of time (months) (Masson et al., 2015), ambient temperature changes happen on a much shorter timescale (hours) and affect the molecular kinetics at the surface of the sensing element (Wang et al., 2010). Humidity affects the sensor by lowering its sensitivity. When water molecules are adsorbed to the surface, they take the place of oxygen on the sensing surface (Qi et al., 2008; Sohn et al., 2008). The water molecules act as a barrier to other molecules interacting with the tin oxide.

To account for the effect of temperature and humidity, previous studies have used compensation factors in the calibration equation. These formulae have had varying degrees of success and ease of implementation (Bastviken et al., 2020; Collier-Oxandale et al., 2018; Eugster & Kling, 2012; Masson et al., 2015; Peterson et al., 2017; Van Den Bossche et al., 2017). Eugster and Kling (2012) conducted the first extensive study demonstrating that modern MOS sensors were capable of measuring ambient level changes in $CH_4$ concentrations. They used manufacturer data to generate a calibration formula to take temperature and relative humidity into account (Eugster & Kling, 2012). This method was appropriate for their study, which considered relative changes in $CH_4$ concentrations; however, individual sensor units have slightly different responses to temperature and humidity. Spinelle et al., (2015) developed a calibration method specific

to individual sensors, which has been followed by several other studies (Collier-Oxandale et al., 2018; Peterson et al., 2017). Collier-Oxandale et al. (2018) and Peterson et al. (2017) used a reference instrument co-located in the field for two weeks with the MOS sensor to calibrate the sensor. The compensation factors used in calibration are adequate and allow a sensor to be used for long-term monitoring, as long as the compensation includes a factor for sensor baseline drift over time. However, they are not conducive for use in a large-scale distributed network, as taking a reference instrument into the field is not practical for many locations. With changing seasons, the calibrated compensation factors could change over time requiring additional calibration periods throughout the year. Van den Bossche et al. (2017) developed a calibration formula that accounts for temperature and humidity effects to use MOS sensors for atmospheric $CH_4$ measurements. Their validation data showed that when temperature and humidity were kept constant in a laboratory environment, the uncompensated sensor response provided a more accurate concentration estimate than the calibration formula did.

In summary, scientific and industrial $CH_4$ monitoring on a large scale requires low-cost, accurate $CH_4$ detectors that can be deployed at scale in the field. Previous research suggested that environmental parameters such as temperature and humidity influence sensor response and that controlling those parameters could improve sensor response.

### 1.6 Research Objectives

This thesis seeks to evaluate the potential of MOS sensors for trace gas monitoring by assessing their performance under laboratory and field conditions and then evaluating the potential of these sensors and the controlled environment for industrial applications.

The thesis specifically focuses on the following objectives.

1. Conduct controlled laboratory testing
    a. Demonstrate sensor resolution better than 500 ppm as stated by manufacturer specifications;
    b. Evaluate major factors influencing sensor response.

2. Develop and test an environmentally controlled enclosure MOS $CH_4$ sensor:
    a. Evaluate sensor resolution;
    b. Evaluate environmental controls;
    c. Evaluate sensor performance inside of an environmentally controlled enclosure.

3.) Test sensor and enclosure in the field to evaluate industrial applications with a focus on the evaluation of the sensor potential for leak detection.

# CHAPTER 2 METHODS

## 2.1 Sensor

The sensor used to measure $CH_4$ concentrations in this research was a MOS sensor of the type TGS2611-E00 (~$15 USD from Figaro USA Ltd., Arlington Heights, Illinois, United States). The TGS2611-E00 model was chosen because it includes a filter cap to remove other oxidizable gases that could cause cross sensitivities described in a previous study (Wang et al., 2010). The $CH_4$ sensor was equipped with a dedicated temperature and humidity sensor (Telaire ChipCap2, Amphenol, St. Marys, Pennsylvania, United States).

## 2.2 Electronic Set Up and Sensors

Power was supplied to the instrument using a 12V power supply. The 12V supply was then divided and connected to step down voltage regulators (PYB10-Q24-S3 and PYB15-Q24-S5, CUI Inc., Tualatin, Oregon, United States), which were used to supply 3.3 V and 5 V to the electronic components. The Figaro TGS-2611 sensor element was mounted on a circular printed circuit board (PCB) along with a fixed resistor (R1) (Figure 2). The variable resistance of the metal oxide of the sensor and fixed resistor R1 formed a voltage divider, the output of which was a voltage that could be measured by an analog-to-digital converter. The ChipCap2 digital temperature and humidity sensor were also mounted on this PCB. This allowed the temperature and humidity to be measured very close to the opening of the TGS-2611. The sensor has an integrated heating element element. This heating element increases the temperature of the $SnO_2$ layer so that oxygen can bond to it.

The sensor module was connected to a control board, consisting of a Teensy 3.2 microcontroller, and support circuitry (PJRC.COM Llc, Sherwood, Oregon, United States) as shown in Figure 2. The board reads the $CH_4$-proportional voltage through a 16-bit analog-to-digital converter input and also reads the temperature and relative humidity sensor using an $I^2C$ serial interface. These values were formatted into a text data stream and were both transmitted using an RS232 serial connection and stored internally on a microSD card.

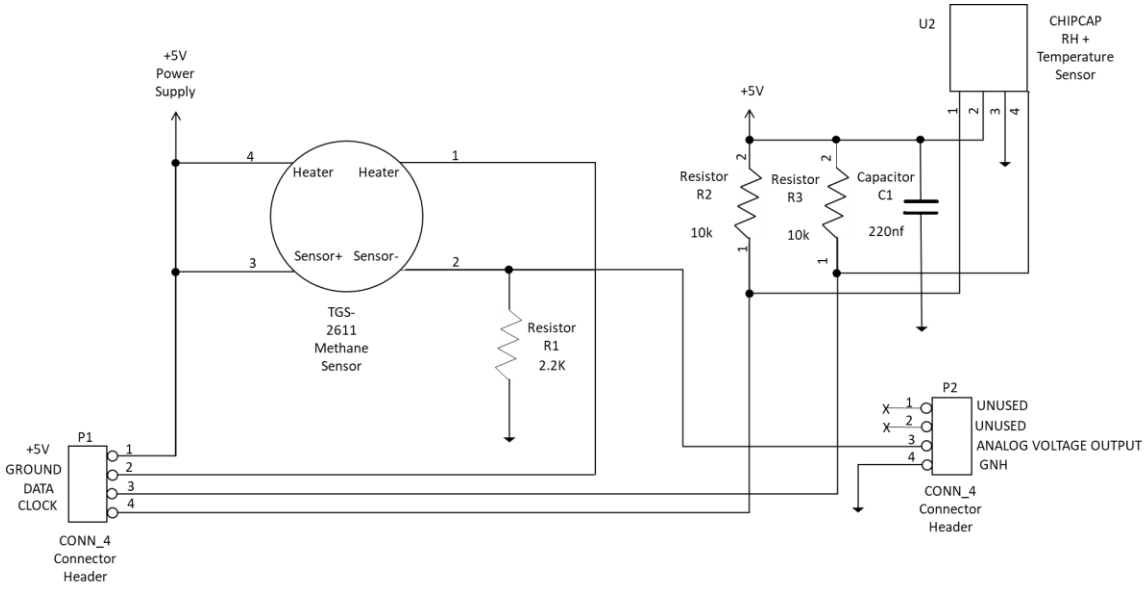


Figure 2 $CH_4$ sensor board electronic configuration. P1 and P2 are the terminals on either side of the board. Leads are used to connect both in the same connector that connects to the loggerboard where power, data, and the clock signal are transmitted.

### 2.3 Laboratory Testing

Laboratory testing was conducted to evaluate the sensor's ability to measure $CH_4$ concentrations as well as its performance under a variety of environmental conditions. The manufacturer of the MOS sensor lists 500 ppm as the lower detection limit of the sensor, but previous research has shown the sensor to be able to measure $CH_4$ at

significantly lower concentrations (e.g. van den Bossche 2016). The first laboratory testing was conducted to assess the detection limit and to generate a concentration calibration. The laboratory testing was designed to be conducted with stable temperature, humidity, and gas concentrations during each treatment.

Five $CH_4$ sensors were mounted inside of a small enclosure, along with an oxygen sensor (O2-A2, Alphasense, Essex, United Kingdom). Five sensors were chosen to allow inter-unit differences to be reviewed. Three gas standards were blended to achieve varying levels of $CH_4$ concentration (2 ppm, 4 ppm, 10 ppm, 20 ppm, 40 ppm, and 80 ppm as shown in Figure 3) with a constant amount of oxygen using a gas blender (GB-103, MCQ Instruments, Rome, Italy), which controlled the composition and flow rate of the sample gas. This gas stream was conditioned to change the relative humidity using an RH Generator (V-Gen Dew Point/RH generator model 1, InstruQuest, Coconut Creek, Florida, United States). The outlet of the RH Generator was connected to the sensor enclosure as shown in Figure 3. The external temperature and RH measurement option was used, and the external sensors were installed in the sensor enclosure using cable glands. The sensor enclosure was installed inside a temperature-controlled chamber (123C, TestEquity LLC., Moorpark, California, United States) (Figure 3).

The outlet of the sensor enclosure was initially connected with a T-fitting to the reference analyzer. The reference analyzer used was the G2508 (Picarro Inc., Santa Clara, California, United States). The reference instrument also has an internal pump, which pumps at a lower flow rate than the gas blender. Thus, the T-fitting was used to avoid any pressure build ups. PTFE tubing (Cole Parmer Instrument Company, Montreal, Quebec,

Canada) was used to connect between devices. At higher humidity levels, condensation would form when the outlet exited the environmental chamber, and a water trap was used to prevent any water from entering the analyzer.

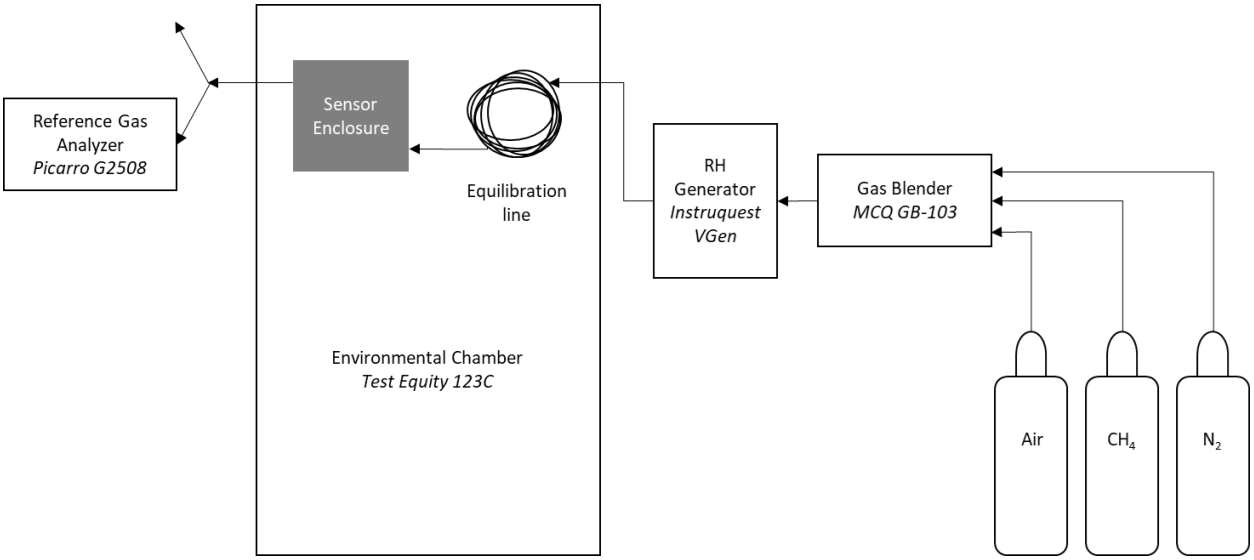


Figure 3 Test configuration showing the gas flow from tanks to the gas blender where varying $CH_4$ concentrations were mixed, to an RH generator where the gas stream was humidified to different relative humidity levels, then into the environmental chamber for varying temperature with a long equilibration line before entering the sensor enclosure. At this point, the gas composition was analyzed, and excess gas was released.

### 2.3.1 Test Parameters

To achieve varying $CH_4$ concentration levels with a constant amount of oxygen, a gas blend with compressed air, a $CH_4$ gas standard, and nitrogen gas were used. The amount of compressed air was held constant in each test, and $CH_4$ and nitrogen were varied to achieve different levels of $CH_4$ with a consistent amount of oxygen to ensure comparability between tests. The laboratory testing was set up as shown in Figure 3 and the intended test parameters are shown in Figure 4.

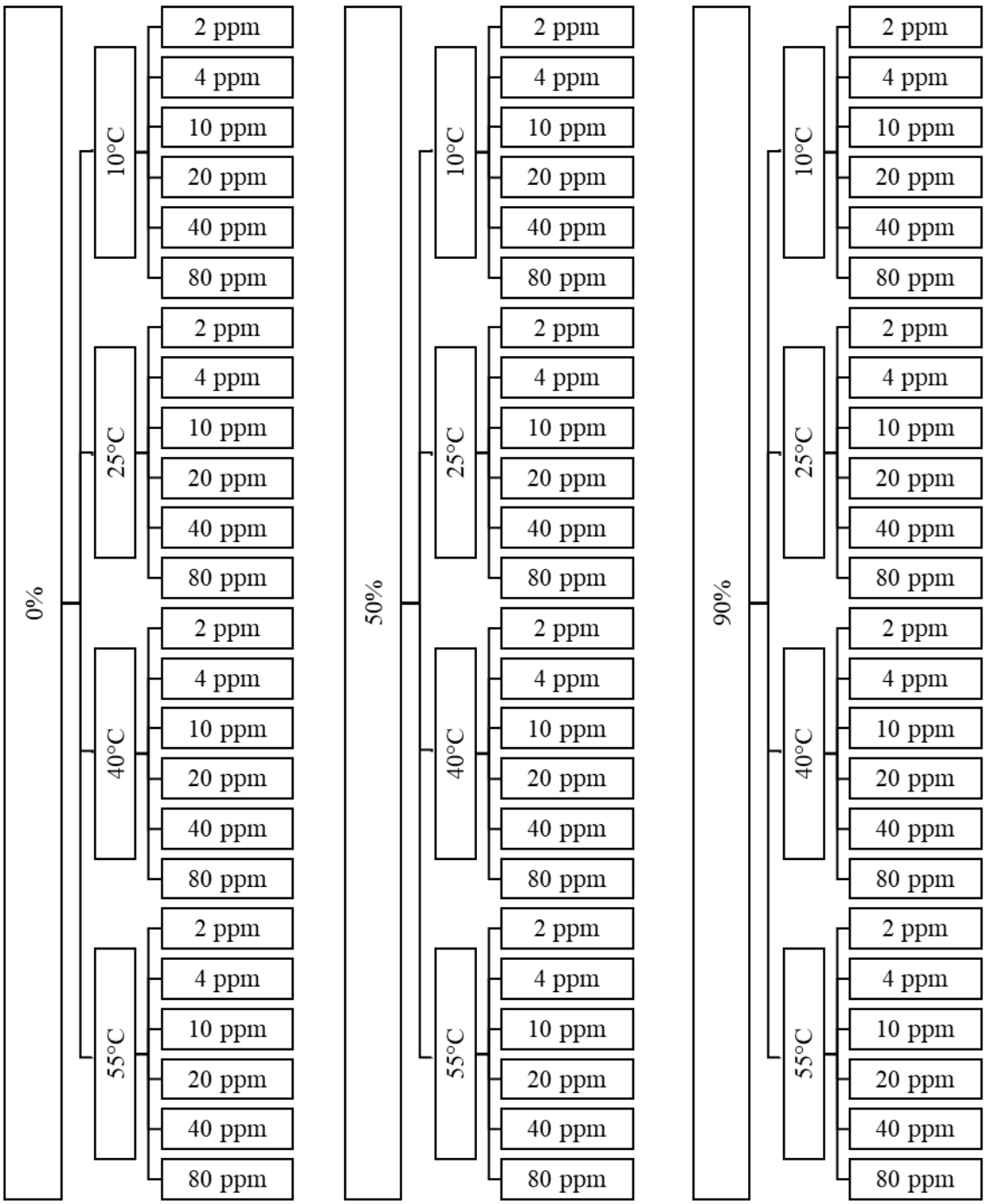


Figure 4 Testing configuration for the MOS sensor for different relative humidity, temperature, and $CH_4$ concentrations.

All parameters from the manufacturer's data sheet with known influences on sensor response were considered in developing the test plan. These parameters include oxygen concentration, organic vapors, dusts and oil mist, silicone, and alkaline metals (Figaro

Inc., 2012). All test materials and enclosures were reviewed for possible cross contamination with known influences, such as silicone, which was avoided, and all enclosures were tested for off gassing. In addition to the test parameters above, oxygen levels were also considered in the test. Different oxygen levels of 10%, 15% and 17% were also part of the testing, but later when considering practical applications in outdoor settings, it was determined that variations in oxygen levels would be negligible and only the results of the 17% oxygen tests were used.

### 2.4 Environmentally Controlled Enclosure Design

Based on the laboratory testing and literature review, it was hypothesized that a controlled environment would improve the accuracy of the sensor and result in consistent calibration results. An environmentally stabilized enclosure with low-cost, low-power sensors was designed and built iteratively in three phases. Each of the three designs consisted of humidity and temperature control hardware, an array of sensors, sample flow control hardware, and electronic controls. To minimize power consumption and overall costs, simple hardware with minimum moving parts were chosen.

#### 2.4.1 Humidity and Temperature Control

Humidity and temperature control were achieved with a combination of hardware components and firmware control logic (Figure 5). A simple heater was determined to require less power than a cooling mechanism. Dehumidifying the sample gas was determined to be more practical than humidifying the sample gas in a continuous monitoring device. Humidifying a gas sample would require a water reservoir, which in turn would require more frequent maintenance than dehumidifying equipment. The sensor box was deployed in Nova Scotia, which is representative of a typical temperate

climate where future deployments could take place, and was designed to have a temperature above the maximum average daily air temperature and a relative humidity lower than the average daily level. The mean daily air temperature in Nova Scotia ranges from approximately -10°C to 25°C, and the average relative humidity ranges from approximately 60% to 90% (Environment Canada, 2018). A higher temperature and lower relative humidity were chosen based on the practical limitations described above as the simplest way to create a stable measurement environment. Additionally, in the initial sensor testing, the tests conducted at lower humidity levels appeared to have better resolution.

The target temperature was set to 35°C ± 1 °C, and the target relative humidity was set to 0%. The targets were chosen based on the previous testing. The temperature in the sensor box was controlled using heat pads, ceramic tiles, a long equilibration line, and insulation. The heat pads were 5V resistive heaters (Rb-Spa-717, RobotShop Inc., Mirabel, Quebec, Canada). The ceramic tiles (XL25, t-Global Technology, Lutterworth, Leicestershire, United Kingdom) were used as thermal mass to help regulate the temperature near the sensors and buffer sudden changes in the sample gas temperature. Two types of insulation were used in the sensor box. Thin Aerogel insulation (Cryogel X201, Aspen Aerogels Inc., Northborough, Massachusetts, United States) was used around the enclosure containing the sensors, and the outer enclosure was lined with a closed cell polyethylene foam insulation (Nomafoam, Nomaco Inc., Zebulon, North Carolina, United States). Aerogels have some of the lowest thermal conductivity values so they can achieve the same level of insulation as thicker conventional insulation materials (Berge & Johansson, 2012), which saves space inside of the instrument. To

reduce the amount of dust around the enclosure the insulation was covered in aluminum foil. A more economical foam insulation was used around the outer enclosure. To assist with temperature regulation, one of the prototypes included a long polyurethane hose (URTH1-0804, Clippard Instrument Laboratory, Inc., Cincinnati, Ohio, United States), which allowed the sample air to equilibrate inside of the outer enclosure (Figure 5).

(a)

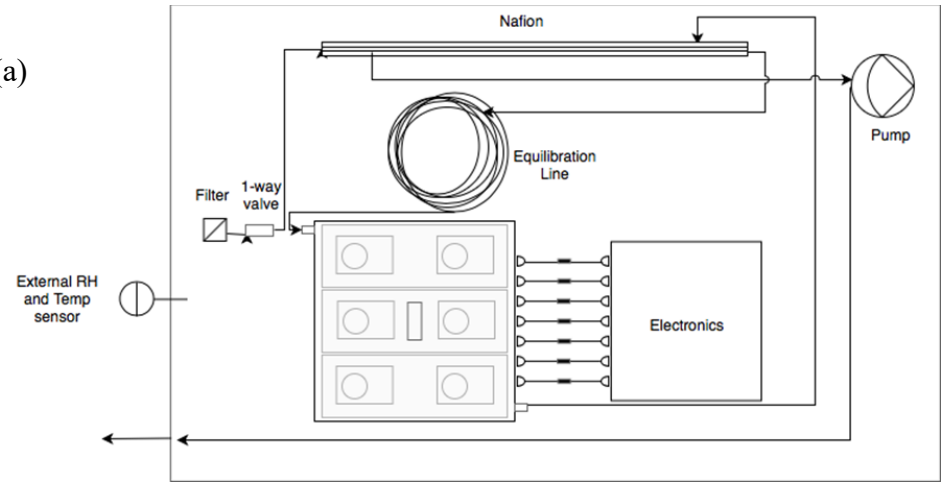


(b)

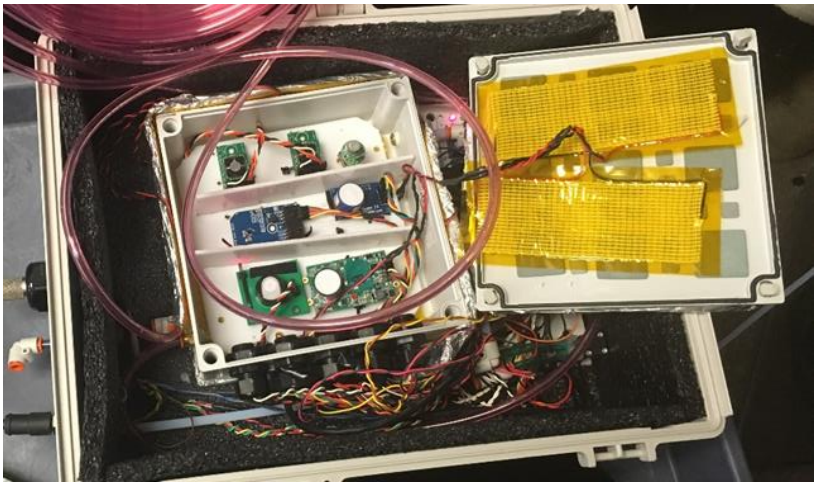

Figure 5 Sensor box final design schematic (a) and photo (b). The additional gas sensors are visible, but their data were not used in this study.

Humidity was controlled using a combination of a Nafion dryer and a desiccant. A Nafion dryer and tubes of desiccant were chosen because they are passive drying methods. The Nafion dryer consisted of a tube of Nafion, a semi-permeable membrane which is highly selective in the removal of water, inside of a larger tube with a cross-flow of a dry gas. The sample gas passed through the Nafion tube, and a dry gas passed through the larger tube. Moisture from the sample line was removed when dry air was passed through the outer tube. The Nafion dryers used were MD-Series dryers for low flow applications (MD-070-12-F-4 and MD-070-48-F-4, PermaPure LLC, Lakewood, New Jersey, United States). The Nafion dryer required a cross flow of a dry gas which travels between the Nafion and the outer tube. To circumvent the need for additional air-drying equipment or gas tanks, the recycled sample gas method was used (Perma Pure

LLC, n.d.). The Nafion dryer was used to remove the bulk of the moisture from the air, and if additional drying was required, the desiccant was used. A tube of Drierite indicating desiccant (W.A. Hammond Drierite Co Ltd., Xenia, Ohio, United States) was used in two of the prototypes.

### 2.4.2 Gas Flow

The gas was drawn through the sensor box using a Schwarzer diaphragm pump (270-EC-Bla, Schwarzer, Essen, Germany). The pump was placed in line after the sensors to limit possible sensor interferences (Figure 5). In one of the prototypes, valves (EWO 3-12, Clippard Instrument Laboratory, Inc., Cincinnati, Ohio, United States) were used to direct the sample gas through different flow paths. A combination of PTFE (RK-06605-32, Cole-Parmer Instrument Company LLC, Montreal, Quebec, Canada) and polyurethane hose (URH1-0804-RDT-050, Clippard Instrument Laboratory, Inc., Cincinnati, Ohio, United States) was used. The other components include a filter (ZenPure, Cole Parmer Instrument Company, Montreal, Quebec, Canada) to trap any liquid water and particulate matter, as well as the sealed polycarbonate inner and outer enclosures (McMaster Carr Supply Company, Atlanta, Georgia, United States). All together the parts were less than $1,000.

### 2.4.3 Prototyping

The components listed above were assembled in three different iterations. Each prototype was designed, fully built, and tested before arriving at the final design. The design and testing prioritized the optimization of humidity and temperature control, while minimizing power requirements and cost. The initial design included six gas sensors to measure $CH_4$, carbon dioxide, carbon monoxide, volatile organic compounds, hydrogen

sulfide, and oxygen, as well as sensors to measure internal and external temperature and relative humidity. The initial iterations were over-designed. The final design combined the best practices from each of the previous prototypes. The final design consisted of an outer and an inner enclosure (Figure 5). The outer enclosure was insulated and contained the Nafion tubing, desiccant, pump, equilibration line, electronics enclosure, and inner enclosure with the sensors. The inner enclosure was heated with the resistive heaters and was insulated and contained the ceramic tiles.

When powered, the sensor box ran through measurement cycles. External temperature and relative humidity were measured. The controller determined whether humidity control was required, and the sample was either dried or went directly through to the equilibration line. The equilibration line was approximately 10 m of ¼ inch outer diameter tubing, allowing the sample to equilibrate to the ambient temperature inside of the outer enclosure prior to entering the sensor enclosure. The sample entered the sensor enclosure where any additional temperature control took place, and when the temperature and relative humidity were stable, the sensor readings were recorded.

### 2.4 Calibration Method and Set Up

The primary goal of the sensor box testing was to demonstrate that an improved calibration can be achieved by stabilizing environmental parameters known to affect the sensor response (temperature and humidity). To validate this concept, tests were conducted to calibrate the $CH_4$ sensor under stable conditions and demonstrate a stable calibration. As with the previous testing, three gas standards were blended to achieve varying levels of $CH_4$ concentration with a constant amount of oxygen using a gas blender. The sensor box was installed inside of the environmental chamber. The outlet of

the gas blender was connected to a calibration line inside of the environmental chamber to allow the gases to reach the temperature of the chamber and then connected to the inlet of the sensor box. The pump inside of the sensor box was bypassed during calibration as the gas blender controlled the flow rate of the gases. The outlet of the sensor box was connected through a T-fitting to the reference analyzer. The reference analyzer used was the G2508 (Picarro Inc., Santa Clara, California). The reference instrument also has an internal pump, but it pumped at a lower flow rate than the gas blender. Thus, the T-fitting was used to avoid any pressure build ups. Polyurethane tubing (URT1-0805, Clippard Instrument Laboratory Inc., Cincinnati, Ohio, United States) was used to connect between devices.

### 2.5.1 Gas Blending

A gas blend with compressed air, a $CH_4$ gas standard, and nitrogen gas were used to achieve varying levels of $CH_4$ concentrations while attempting to maintain a constant oxygen concentration.

The following gas standards were used:

| | |
|---|---|
| Oxygen | Breathing grade air (Praxair I BR-T) |
| Methane | 999 ppm $CH_4$, Balance $N_2$ (Praxair NI MER2C-K) |
| Nitrogen | Ultra High Purity Nitrogen (Praxair NI 5.0UH-T) |

The gases were combined to achieve $CH_4$ concentrations between 2 ppm and 80 ppm. Each concentration level was run for one hour and then increased or decreased to the next step over two minutes. A purge gas was run between each test for one hour, and the purge gas had a higher oxygen concentration than the gas blend used in the calibration. A

sample timeseries of these data are shown in Figure 6. The sections between each test with the elevated oxygen were removed for data processing.

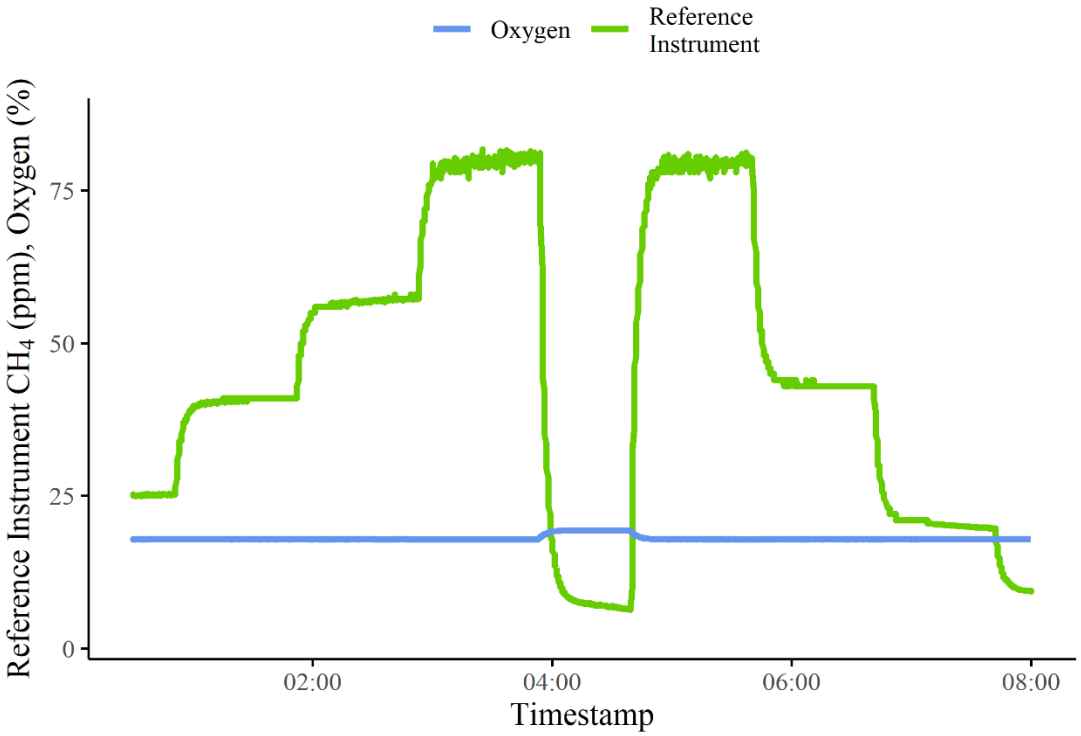


Figure 6 A segment of time between two "tests" showing the change in oxygen concentration and $CH_4$ concentration.

## 2.5 Field Testing

### 2.5.1 Controlled Release Testing

A controlled release test was set up with the reference analyzer in an agricultural field near Bridgewater, Nova Scotia. This testing was conducted between May and June of 2020 when the mean daily temperature ranged from 5°C to 21°C and the relative humidity ranged from 68% to 100%. A tank of 93% $CH_4$ (ME 1.3-TN, Linde Canada Inc. (Praxair), Mississauga, Ontario, Canada) was connected to a flow controller (MCQ, Alicat Scientific, Tucson, Arizona, United States) and then to a plastic release head which

was installed 2 m above ground surface on a wooden support. The release rate was set at points between 4 $m^3$/day and 64 $m^3$/day. The reference analyzer and MOS sensor were installed on a tripod, with the sample inlet at 2 m above ground surface (Figure 7). The MOS sensor was installed downline of the reference instrument in the field. A long equilibration line was used between the reference instrument and the sensor box.

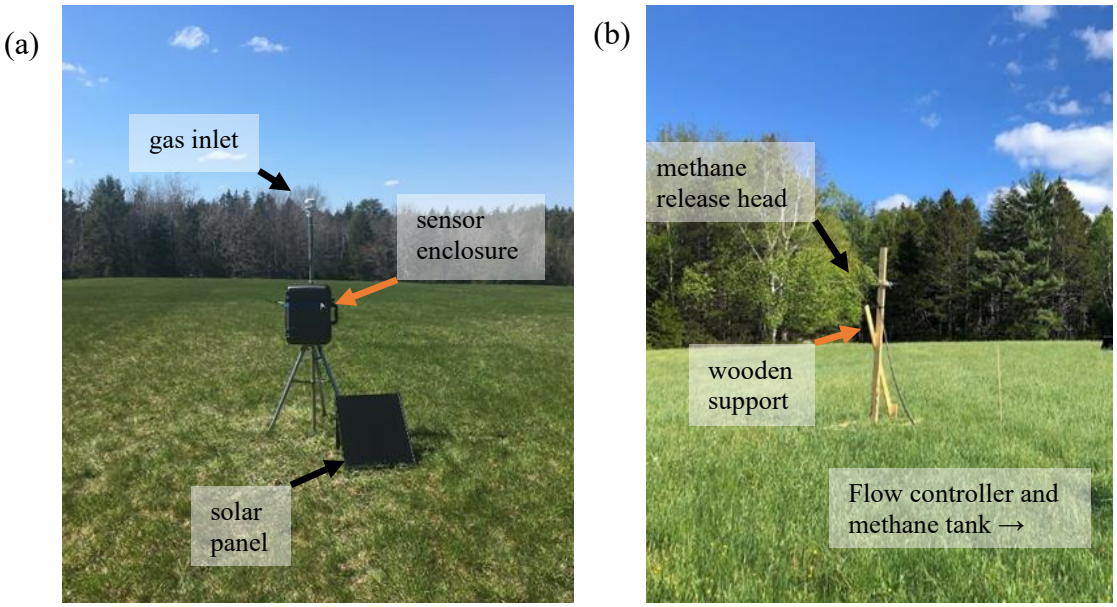


Figure 7 Photos of the instrument (a) and release head (b) set up for the controlled release testing. The flow controller and $CH_4$ tank are not pictured. Photos were taken May 22, 2020.

The release location was moved throughout the test from 8 m to 50 m away from the measurement point to determine optimal measurement conditions. This test was intended to compare a sensor with no environmental controls to a sensor with environmental controls in a field setting.

### 2.5.2 Industrial Monitoring

Following the controlled release, another field trial was conducted at a natural gas compression station to evaluate the sensor for use in an industrial monitoring application with a focus on its ability to detect episodic releases of $CH_4$. This testing was conducted

between June 24 and July 13, 2020, with daily mean air temperatures between 7°C to 25°C and mean relative humidity from 68% to 100%. This site was chosen due to the frequent and sporadic nature of the releases that occur. At this station, transmission vehicles were filled, and at the end of loading, the compressed $CH_4$ in the line was vented.

To minimize dilution effects due to a large internal sensor enclosure volume inside of the sensor box, the low-cost sensor was equipped with a small cap, and it was installed directly inside of the reference analyzer enclosure. The reference analyzer and low-cost sensor were monitored at the natural gas compression station for two weeks.

The reference sensor, MOS sensor, temperature, and relative humidity sensors were installed with an Arduino Leonardo microcontroller (Arduino, Somerville, Massachusetts, United States) to convert the sensor signals for the logger, and a Campbell Scientific datalogger (CR1000X, Campbell Scientific Canada, Edmonton, Alberta, Canada) was also used as a controller for the other components. A cap was machined for the low-cost sensor to reduce the volume. The sensor was plumbed shortly downstream of the reference analyzer and before the pump (SP270, Schwarzer, Essen, Germany), which was used to transport gas from the inlet. The enclosure was installed on a tripod with a 1.98 m mast. The sonic anemometer (Atmos 22, Meter Group, Pullman, Washington, United States) and the gas inlet were situated at the top of the tripod at a height of approximately 2 m and later increased to 4.5 m. The tripod was installed approximately 40 m downwind of the loading station as shown in Figure 8.

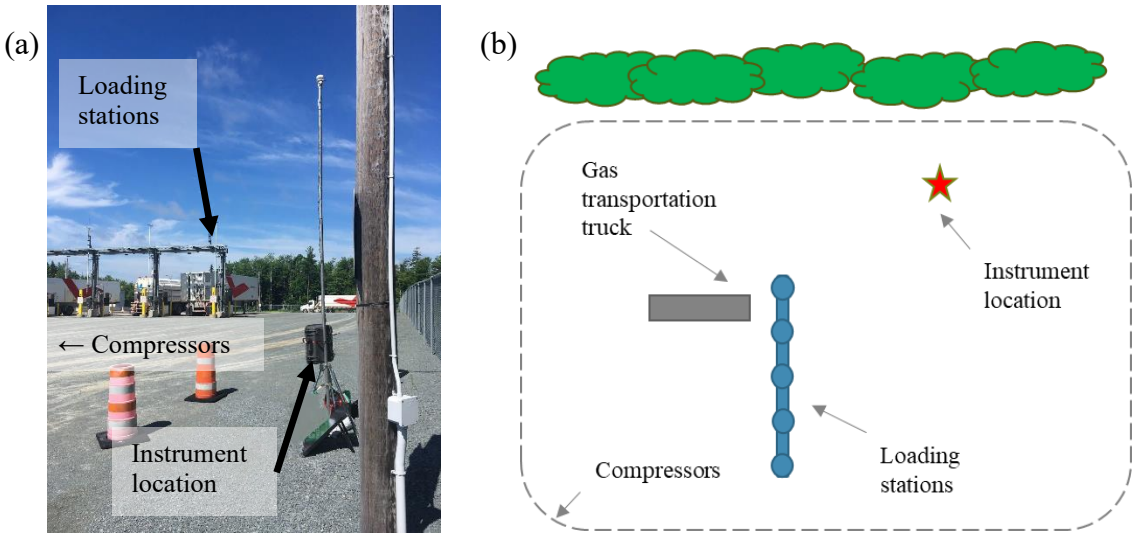


Figure 8 Photos of the instrument (a) and site schematic (b) showing the location of the instrument relative to the source (loading stations). Photo was taken June 30, 2020.

## 2.6 Data Analysis

### 2.6.1 Resistance Ratio

The MOS sensor was configured to report the voltage measured across the semiconductor. The resistance ratio ($R_S/R_0$) is used to evaluate a sensor's sensitivity. It is the ratio of the resistance of the sensor measured in the presence of the gas of interest ($R_S$) to the resistance of the sensor measured in fresh air ($R_0$). Fresh air is defined as air with atmospheric $CH_4$ concentration levels. The resistance is calculated using Ohm's law and the circuit set up (Figure 2).

$$I = \frac{V_C}{(R_S + R_L)} \quad (1)$$

Rearranging for $R_s$ yields:

$$R_S = \frac{(V_C \times R_L)}{V_{OUT}} - R_L \quad (2)$$

where:

$V_C$ = Supply voltage = 5 VDC
$R_L$ = Precision resistor = R1 = 2.2 kΩ
$R_S$ = Variable sensor resistance = resistance measured between points 2 and 3 on MOS Sensor in Figure 2
$V_{OUT} = V_S$ = Voltage measured across precision resistor (R1)

Inserting the known parameter values reduces equation (2) to:

$$R_S = \frac{(5 \times 2.2)}{V_{OUT}} - 2.2 \quad (3)$$

The reference resistance ($R_0$) is calculated using the same formula but with the $V_0$ measured in fresh air (ambient air with no added $CH_4$) as a constant reference voltage:

$$R_0 = \frac{(5 \times 2.2)}{V_0} - 2.2 \quad (4)$$

In the tests, the $CH_4$ present in fresh air varied between 1.7 and 2.3 ppm. Due to the variability in background concentrations, the minimum voltage was used for $V_0$ as described by Bastviken et al. (2020).

### 2.6.2 Data processing – Lab Testing and Controlled Environment Testing

Measurements of temperature (°C) both inside and outside of the sensor enclosure, as well as relative humidity (%), oxygen (%), and $CH_4$ sensor response (V) were recorded by the loggerboard. These data were recorded every 15 seconds and stored as text files on the instrument's datalogger, and serial data files were collected during testing using a serial port terminal with logging capabilities (CoolTerm for Windows). Additionally, data from the other sensors were collected and stored, but were not used in these analyses. Similarly, field data were collected and stored on a data logger.

The reference $CH_4$ concentration (ppm) from the reference analyzer were recorded every 10 seconds and were stored on the instrument's hard drive as text files which were downloaded separately. The data were processed and analyzed using Microsoft Excel 2016 and R 4.0.1 using R Studio 1.3.959 (R Core Team, 2020) to process data, generate plots, and conduct statistical data analyses. The reference analyzer data were time adjusted to account for the time difference between instrument response times as well as the time lag in gas transport between instruments. The time correction was determined by trial and error for the first test and was verified for subsequent tests. This was done by matching the reference instrument's $CH_4$ concentration timeseries curve to the sensor response timeseries curve. Times at which the concentration increased or decreased rapidly were the clearest to identify. For the field testing, the reference analyzer data were stored on the same datalogger, and no time adjustment was required. R (R Core Team, 2020) was used to generate calibration plots using the resistance ratio as calculated using equations (3) and (4) and reference $CH_4$ concentration. Several statistical models were evaluated to determine the best fit, and error analyses (root mean square error) were conducted on each model.

# CHAPTER 3 RESULTS

## 3.1 Laboratory Testing of MOS Sensor

During laboratory testing, the MOS sensor was evaluated for its ability to measure $CH_4$ concentration between 2 ppm and 80 ppm under different relative humidity and temperature levels. The tests were designed to explore sensitivities to the parameters shown in Table 3. Oxygen levels were varied, but, as the atmospheric oxygen levels are not expected to vary in ambient conditions, only results for 17% were considered in the analysis. These parameters were previously described to have an influence on the sensor output; however, prior to this study, their impacts on sensor response had not been robustly quantified.

Table 3: Test parameters for MOS sensor environmental laboratory testing.

| Parameter | Intended levels |
|---|---|
| Relative Humidity (%) | 0 |
| | 50 |
| | 90 |
| Temperature (°C) | 10 |
| | 25 |
| | 40 |
| | 55 |
| | 80 |
| Oxygen (%) | 10 |
| | 15 |
| | 17 |

While the intended testing levels in Table 3 were attempted, the actual testing levels achieved differed. An example of a single test cycle is shown in Figure 9 with a constant temperature and humidity and with the transitions between tests removed for clarity. This test cycle was repeated for five temperatures and three relative humidity levels (Table 3). Unfortunately, due to a gas leak, only the data from the 50°C and 80°C temperature steps are available for the 50% relative humidity test with 17% oxygen.

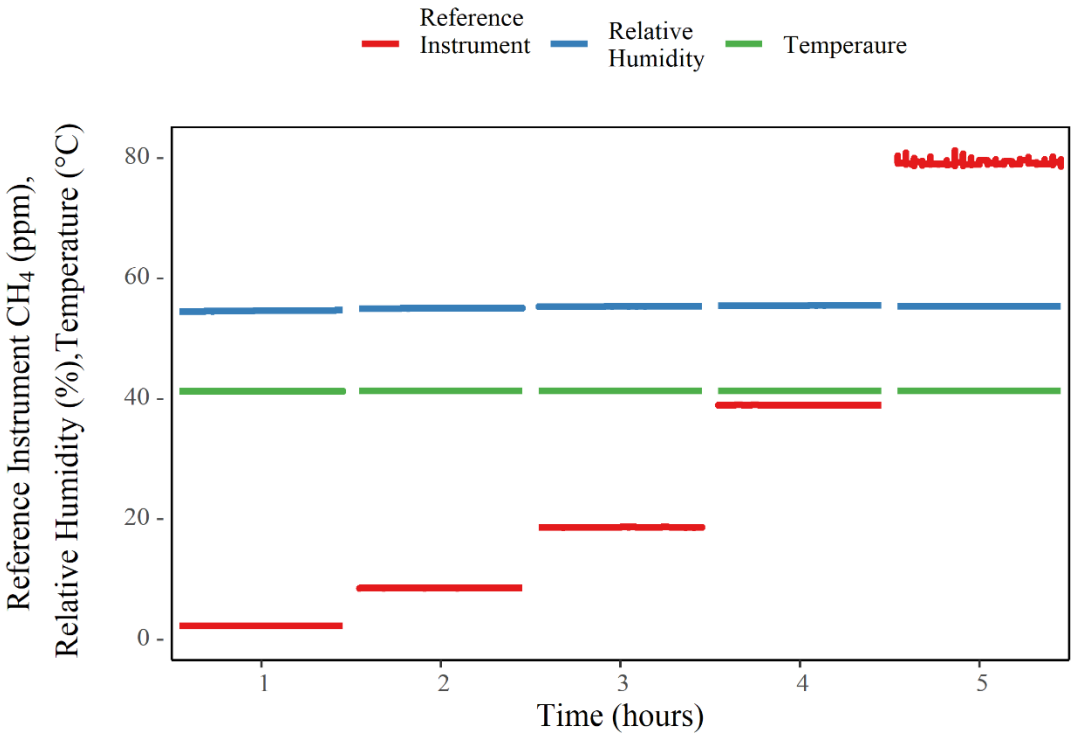


Figure 9 A single calibration test cycle showing the reference instrument $CH_4$ concentration, the relative humidity, and the temperature during the test (see Table 3).

Out of a total of 180 combinations of $CH_4$ concentration, temperature, relative humidity, and oxygen tested (Table 3), only 60 with an oxygen level of 17% were ultimately anlaysed (see also Figure 4). Out of the 60 test combinations, there were only 50 treatments with complete data due to the gas leak mentioned previously. The actual test

data (50 treatments along with two repeated treatment cycles) are shown in Figure 10. The transition time between treatments was filtered out for clarity purposes.

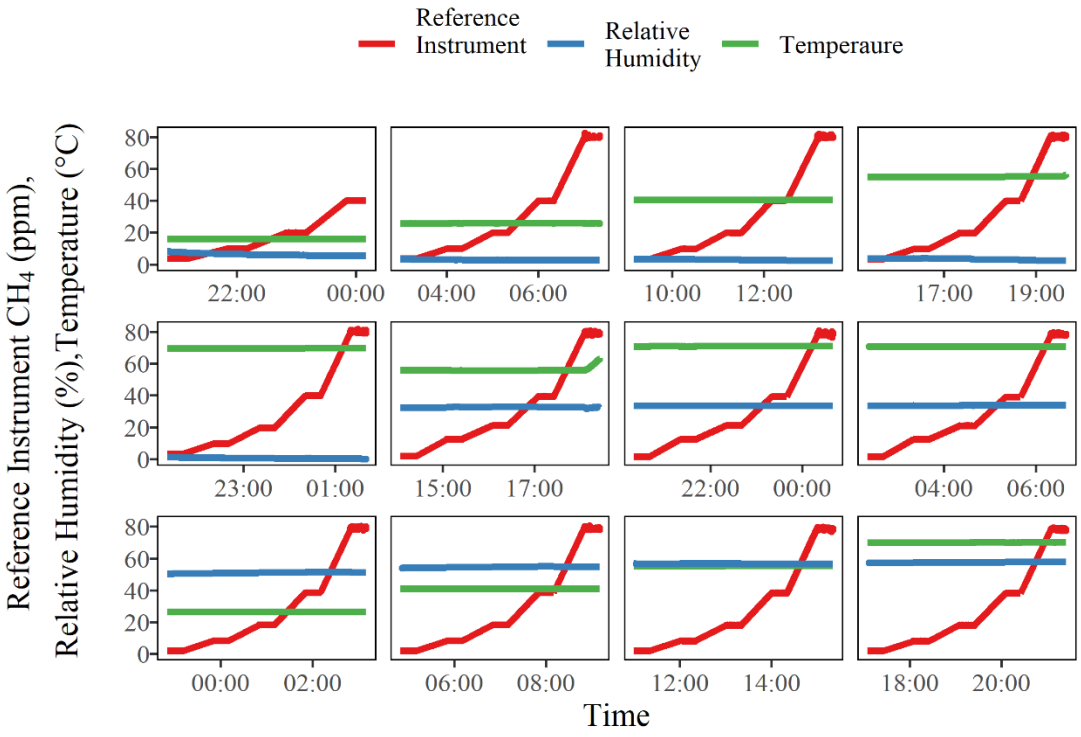


Figure 10 All 50 laboratory treatments used in sensor analysis showing actual environmental conditions. Each plot shows 5 methane concentrations (each of those considered a sensor treatment) and there are two repeated treatment cycles.

### 3.1.1 MOS Sensor Data

The data used to generate a calibration for the sensor are shown below in Figure 11. Each test treatment ran for one hour. A 30-minute segment of data was selected from the centre of each step to avoid transition effects. These 30-minute segments are shown in the plot (Figure 11). The resistance ratio, as calculated using equations (3) and (4), was used in subsequent analyses.

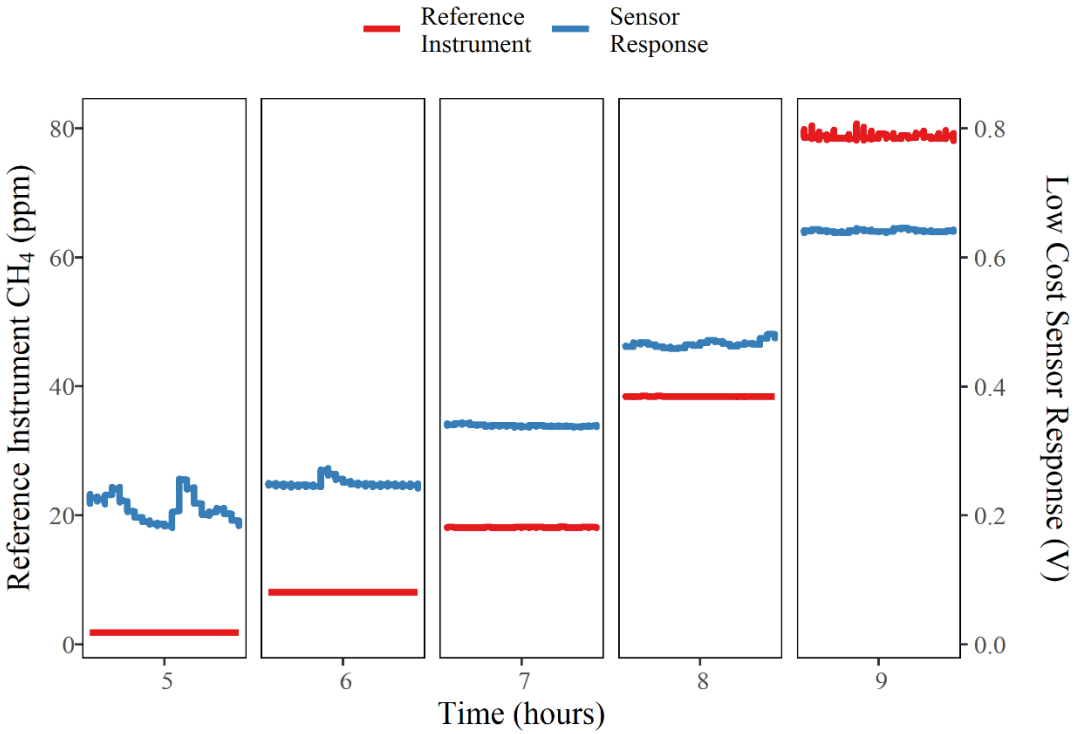


Figure 11 Raw test data from laboratory testing showing the sensor response (voltage, blue, right axes) in different tests compared to the reference instrument's $CH_4$ concentration measurement (ppm, red, left axis). For this test the temperature was 40 °C and the relative humidity was 50%.

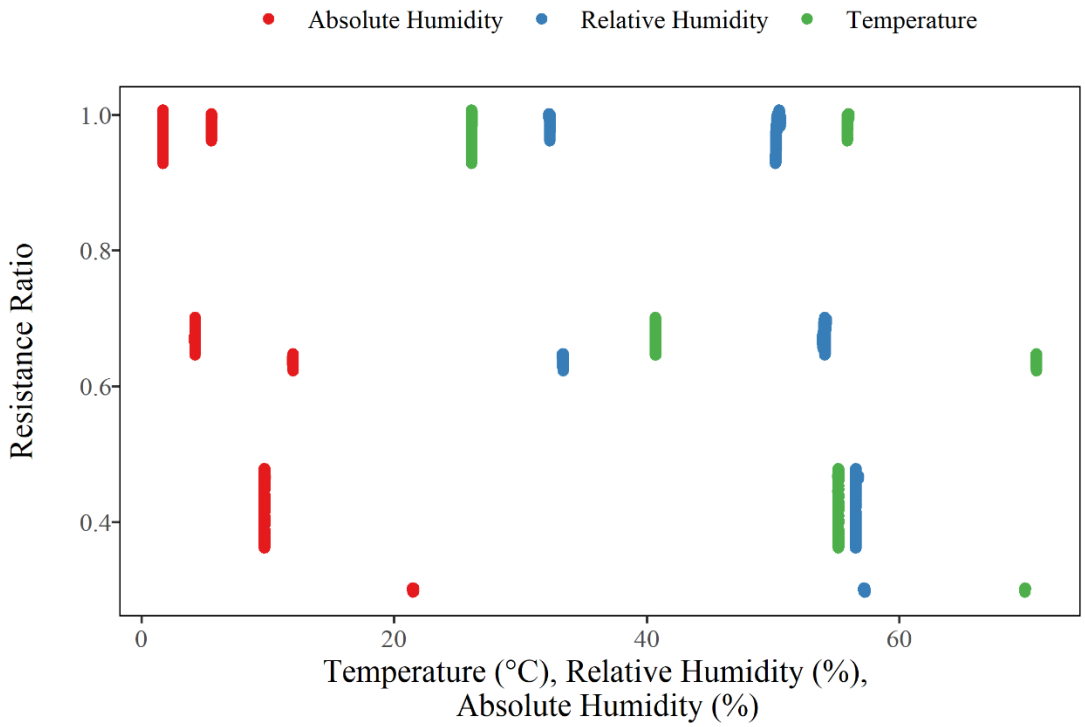


Figure 12 Resistance ratio compared to environmental conditions at a single concentration level (between 1.5 and 1.8 ppm $CH_4$) to demonstrate the influence of temperature and humidity on sensor response.

The initial laboratory testing was successful in demonstrating that the sensor can detect variations in $CH_4$ concentrations less than 500 ppm and in showing that temperature and humidity have an influence on the MOS sensor response (Figure 12). The sensor was able to resolve between approximately 2 ppm and 4 ppm in early tests with low relative humidity. With higher relative humidity, it was more difficult to resolve between the steps at lower concentrations (Figure 13).

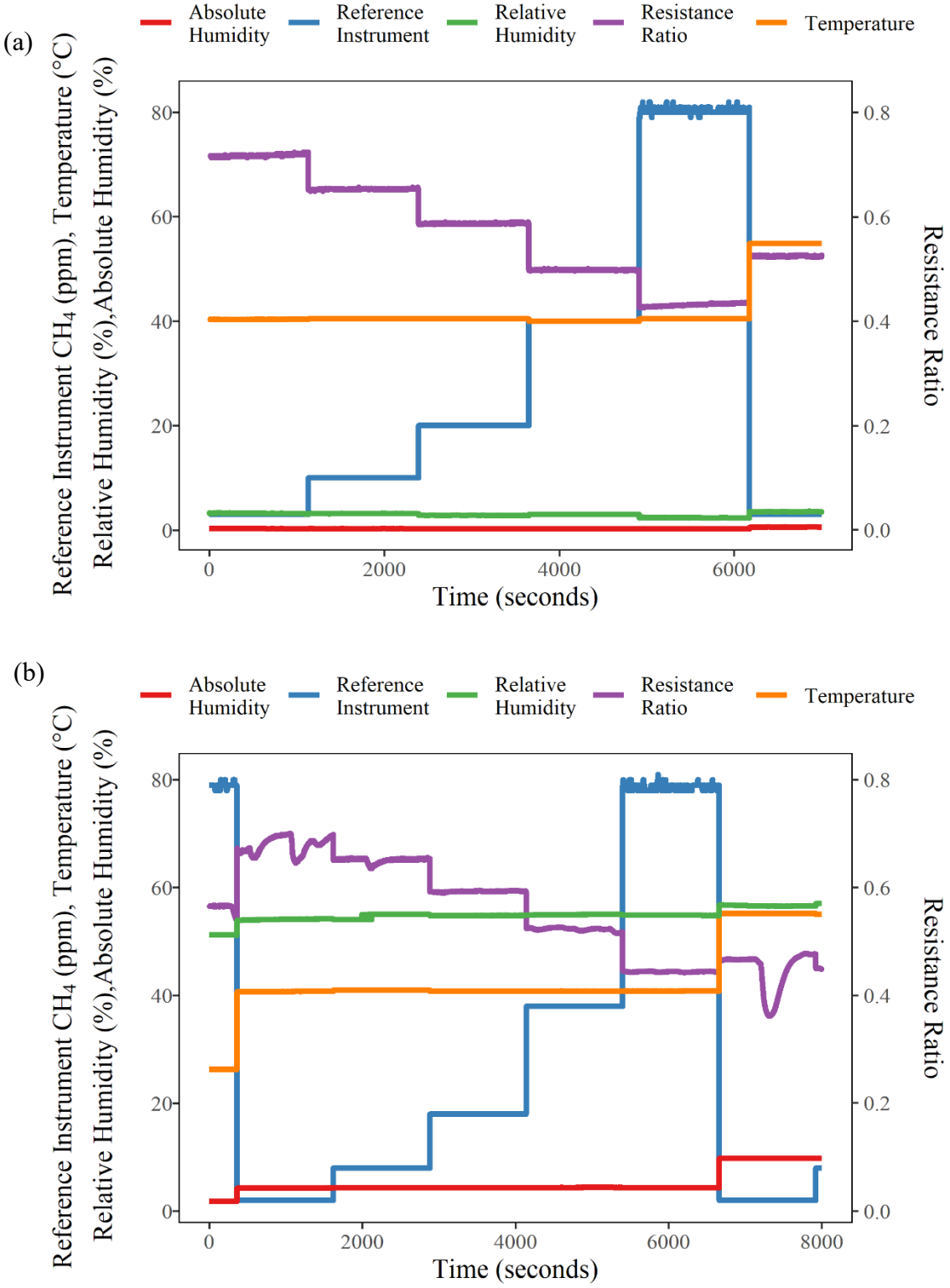


Figure 13 An example of measured $CH_4$ concentration (using the reference instrument) and resistance ratios (using the MOS sensor) in a test with a low relative humidity a) compared to a test with high relative humidity b).

A review of the Pearson correlation coefficients between parameters and sensor response in this testing (Table 4) indicated that absolute humidity had the strongest correlation, demonstrating that absolute humidity was the most important variable to control. The correlation results indicate that the sensor's response more closely indicated changes in the environmental parameters than it did for changes in the methane concentration. The Pearson correlation agrees with the field observations later seen in Figure 19.

Table 4: Pearson correlation between the MOS sensor response and temperature, relative humidity, and reference $CH_4$ concentration for all test treatments.

| | **Temperature (°C)** | **Relative Humidity (%)** | **Absolute Humidity (ppm)** | **Reference Instrument $CH_4$ (ppm)** |
|---|---|---|---|---|
| Sensor Response (V) Pearson correlation | 0.58 | 0.80 | 0.88 | 0.22 |
| *P*-value | < 0.0001 | < 0.0001 | < 0.0001 | < 0.0001 |
| n | 80639 | 80639 | 80639 | 80639 |

During the laboratory testing, some of the targeted relative humidity parameters were not reached, for example the intended 90% relative humidity step was measured at closer to 60%. This was likely partially due to the heating element on the sensor increasing temperature near the sensor. There was also variability between tests completed on different days. Temperature varied at most approximately 2°C between tests, relative humidity varied up to 10%, and $CH_4$ concentration varied up to 2 ppm between tests. One additional issue was in timing the three different instruments used to control temperature, relative humidity, and gas concentration. Each of these instruments has its own internal clock, and each was programmed separately. Though buffer time was included between

tests, there were a few cases of the timing of the instruments not lining up, resulting in data loss.

## 3.2 Laboratory Testing of Environmentally Controlled Enclosure

At the time of the initial testing, limited literature was available to demonstrate the potential for these sensors to be used in ambient monitoring applications. The laboratory testing with controlled environmental conditions demonstrated that the sensor was potentially capable of a resolution much lower than the manufacturer specifications, particularly when humidity is low, and revealed the sensor's sensitivity to changes in temperature and humidity. The sensor box was developed based on those results. The following results are for the calibration testing described in section 2.4. The sensor was inside of the sensor box, but the environmental chamber and dry calibration gas were used to attempt to calibrate the sensor inside of the sensor box and to evaluate the calibration.

### 3.2.1 Environmentally Controlled Enclosure Data

The data were pre-processed as they were for the initial laboratory testing with the time adjusted between instruments. The relationship between the sensor resistance ratio and the reference concentration was used to calibrate the sensor (Figure 14).

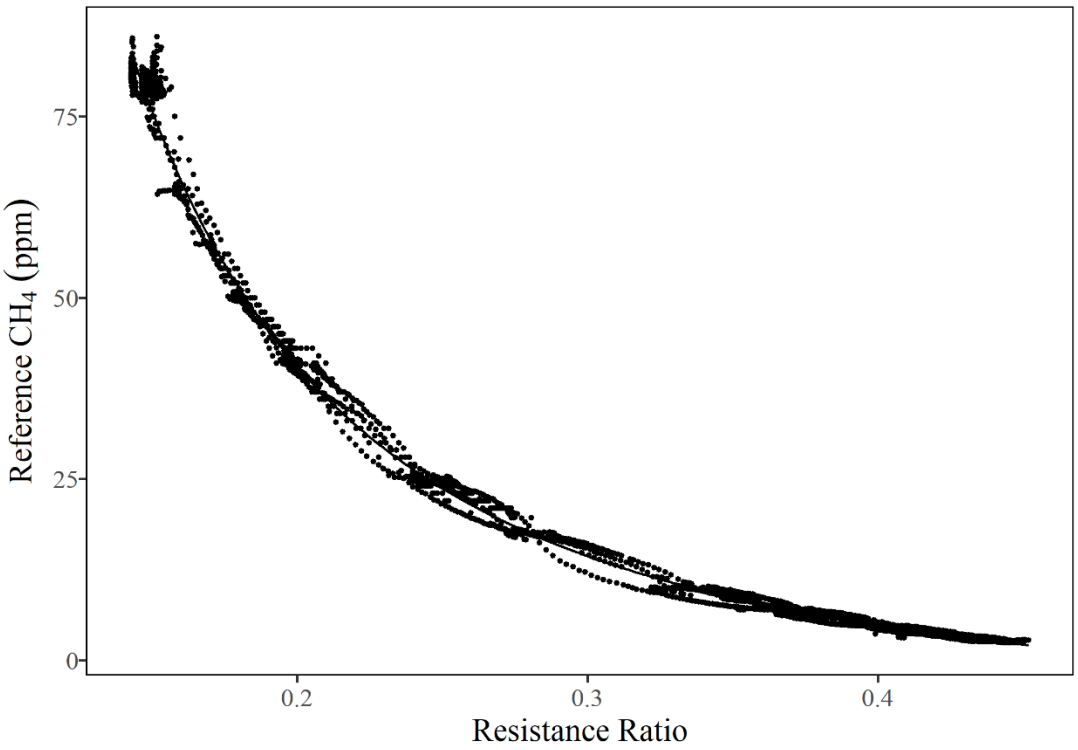


Figure 14 Sensor box calibration curve (reference concentration vs. resistance ratio) at a single temperature (25°C) and humidity (0%). The data were time adjusted, but some hysteresis was still evident.

Using the test data from a single temperature and humidity (i.e., as an example for a controlled environment measurement), several different calibration models were evaluated. The results of the various calibrations are summarized in Table 5. A power-fit produced the best fit (lowest root mean square error) and thus was applied to the resistance ratio and reference concentrations as shown in Figure 15.

Table 5: Calibration models evaluated for the sensor box calibration (RMSE = root mean square error).

| Model | Equation | RMSE (ppm) |
|---|---|---|
| Linear | $C = -96.47 \cdot \frac{R_S}{R_0}$ | 9.02 |
| Log-Linear | $\log(C) = -5.00 \cdot \frac{R_S}{R_0}$ | 2.95 |
| Power | $C = 5.01 \cdot \frac{R_S}{R_0}^{-2.49}$ | 2.41 |
| Power | $C = 10.64 \cdot \frac{R_S}{R_0}^{-1.88} - 8.46$ | 1.32 |
| Exponential | $C = 416.52 \cdot e^{-5.15 \cdot \frac{R_S}{R_0}}$ | 1.66 |
| Exponential | $C = 456.51 \cdot e^{-5.45 \cdot \frac{R_S}{R_0}}$ | 1.57 |
| Polynomial | $C = 229.21 \cdot \frac{R_S}{R_0}^2 - 401.77 \cdot \frac{R_S}{R_0} + 179.18$ | 3.55 |

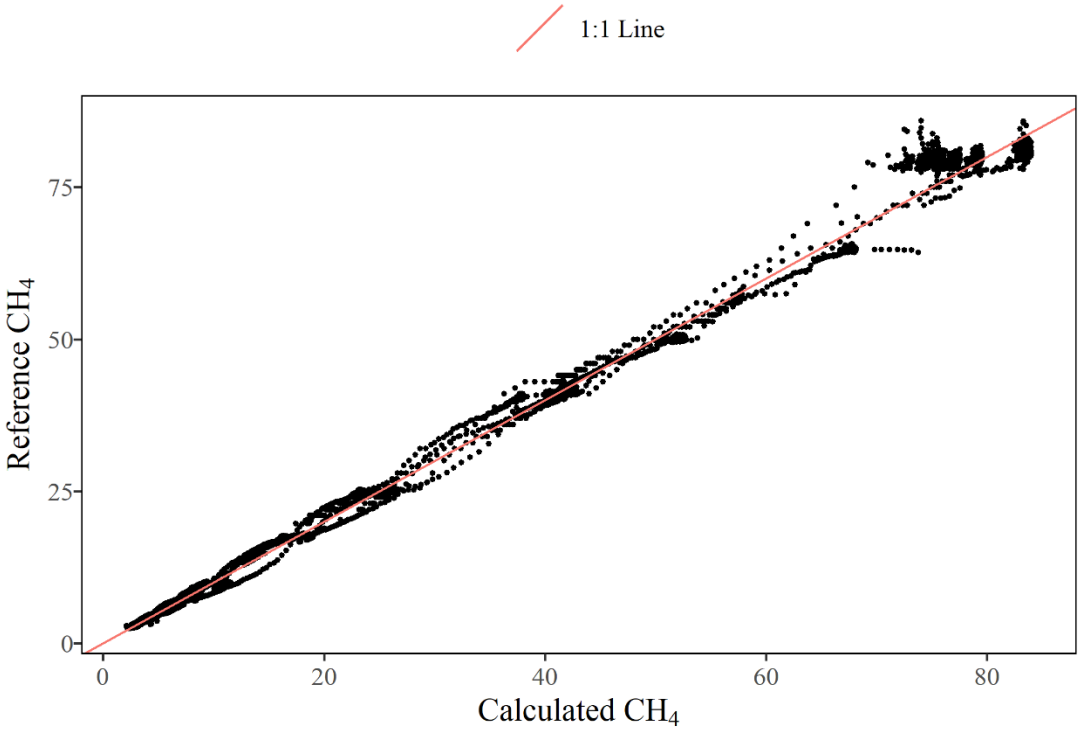


Figure 15 Sensor's calculated CH4 concentration from the power function $C = 10.64 \cdot \frac{R_S}{R_0}^{-1.88} - 8.46$ (Table 5) and the reference CH4 concentration.

### 3.3 Field Testing of MOS Sensor and Environmentally Controlled Enclosure

A direct field comparison between a reference instrument and the sensor box was attempted; however, a design flaw was discovered while studying the instrument at an industrial site. Industrial emissions, particularly atmospheric measurements of above-ground oil and gas facilities are measured as short peaks by a $CH_4$ sensor both due to the nature of the emissions (process based short releases) and due to changing wind directions. The reference instrument was able to capture the short pulses. However, the MOS inside of the sensor box was contained within a large measurement volume, so the short pulses were diluted by the time they arrived at the sensor. Unfortunately, those diluted pulses could not be distinguished from the background concentration (Figure 16).

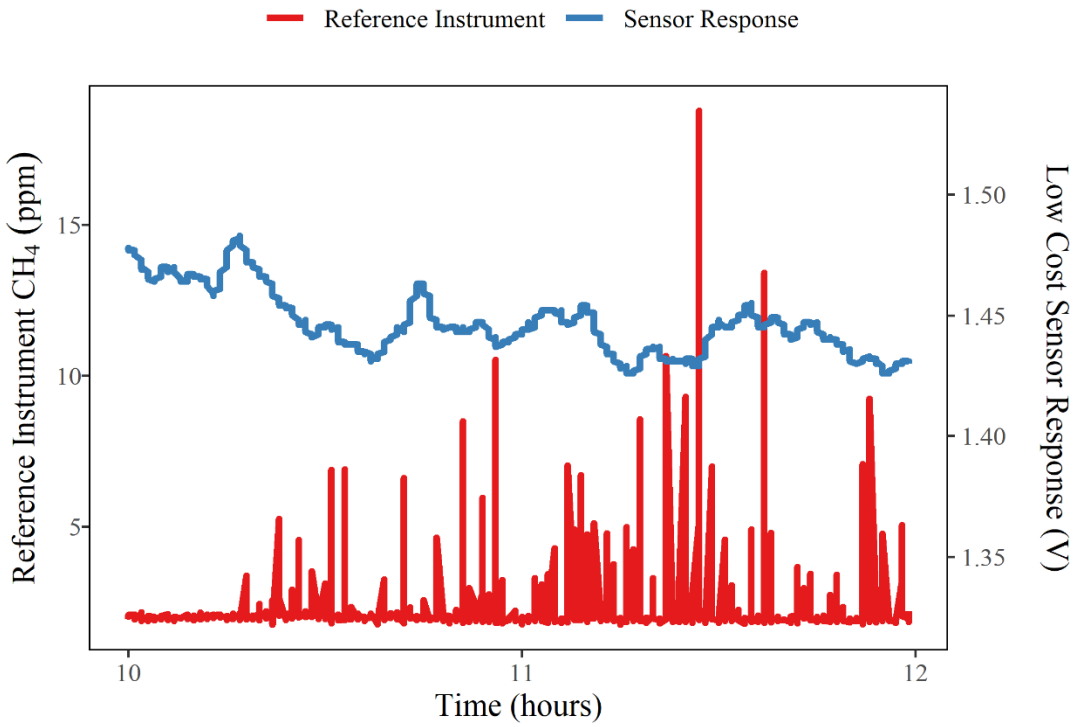


Figure 16 Diluted low-cost sensor response inside the sensor box (blue) as compared to reference instrument (red). The sensor box was not able to detect the methane pulses.

While application and design constraints limited a full field test, the ability to recreate the same conditions in the field as were present in the lab indicates the potential of a similar sensor performance if the dilution effect were not present (Figure 18). While field conditions can bring unexpected parameters into consideration, we can reasonably assume that the performance would be at least on the same order of magnitude as the laboratory results.

The sensor box maintained a stable temperature and humidity during periods of variable ambient conditions. The temperature range inside of the sensor box was only 2.5°C, compared with 11.4°C outside. More importantly, the humidity range decreased by 700% and remained below 3000 ppm while ambient humidity fluctuated between 100,000 ppm and 40,000 ppm (Figure 17).

(a)

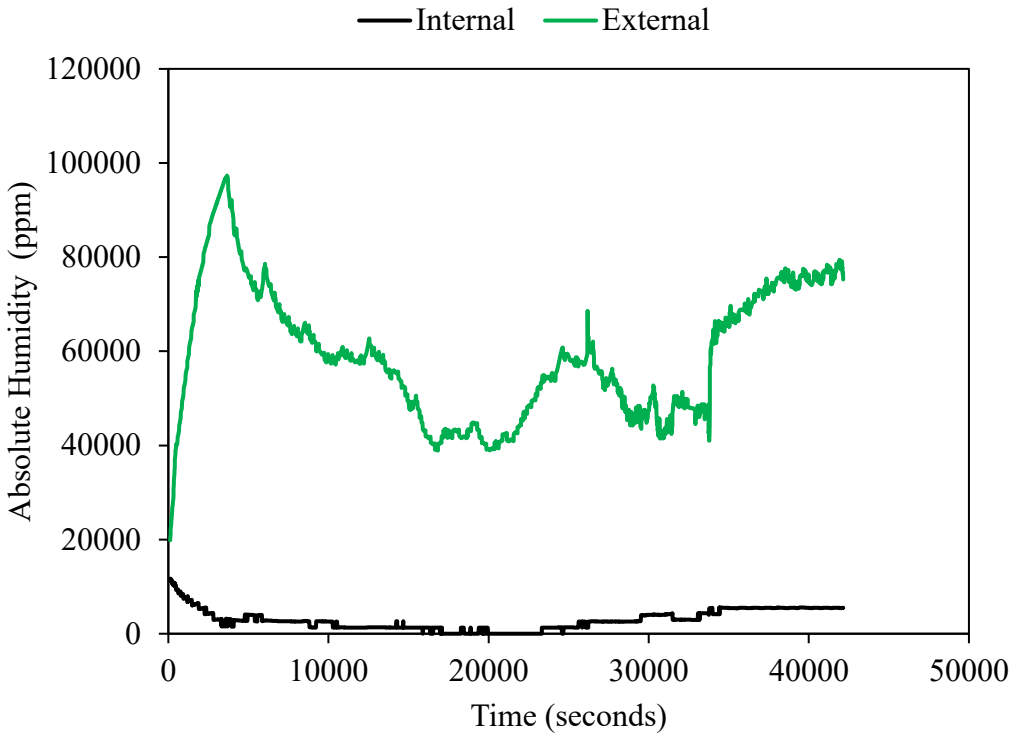


(b)

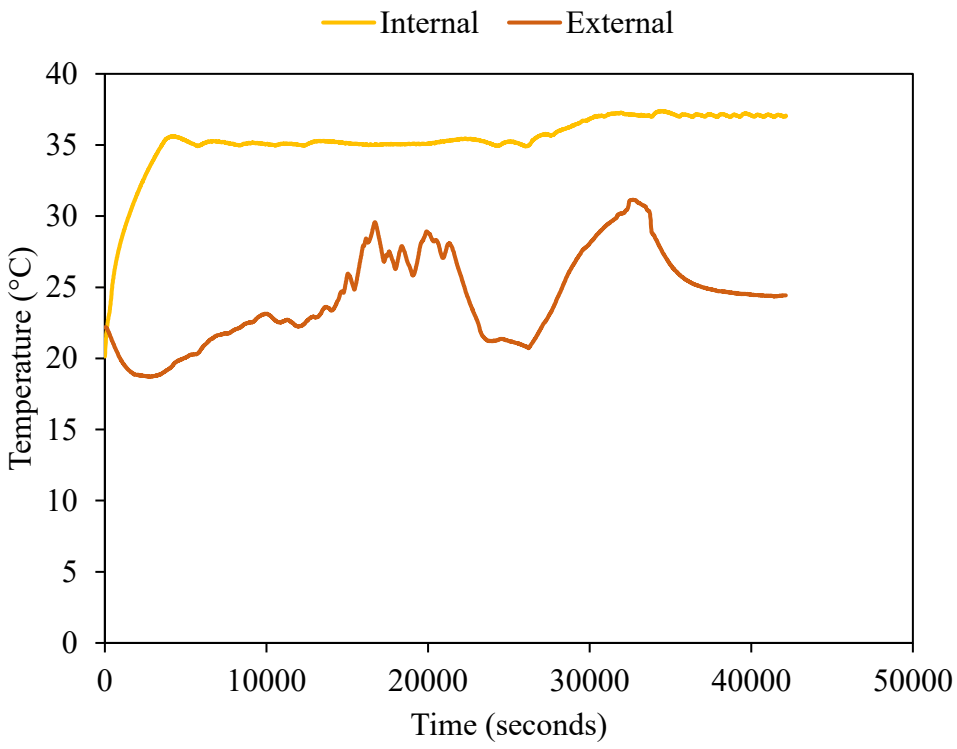


Figure 17 Sensor box's environmental control performance. The reduction of absolute humidity is shown in a), and the temperature stabilization performance is shown in b). Note: The increase at t=0 is the instrument being turned on and the pump bringing in outside air.

Table 6: Sensor box field performance. Data tabulated for time after start-up period (t=5000s).

| | Temperature (°C) | | Relative Humidity (%) | | Absolute Humidity (ppm) | |
|---|---|---|---|---|---|---|
| | Internal | External | Internal | External | Internal | External |
| Min | 34.91 | 19.72 | 10.00 | 29.00 | <1 ppm | 388645 |
| Max | 37.40 | 31.15 | 14.00 | 54.00 | 5579.11 | 82581 |
| Range | 2.49 | 11.43 | 4.00 | 25.00 | 5579.11 | 43717 |

The sensor box was able to control the temperature to within 2.5°C and control the relative humidity within 4% (Table 6). Compared to the lab calibration with a range of 0.2°C for temperature and 1% for relative humidity range during the tests, we would not expect the same performance from the sensor (RMSE 1.34 ppm, see Table 5). In the absence of adequate field comparison data for the sensor, similar lab test results were compared. A lab test of the sensor with relative humidity ranging from 0 to 50% and temperatures ranging from 15 to 40°C had an RMSE of 25.9 ppm when calibrated using a power function (Figure 18a). A lab test with a temperature range of 45 to 47°C and a relative humidity ranging from 1% to 8% had an RMSE of 3.4 ppm (Figure 18b).

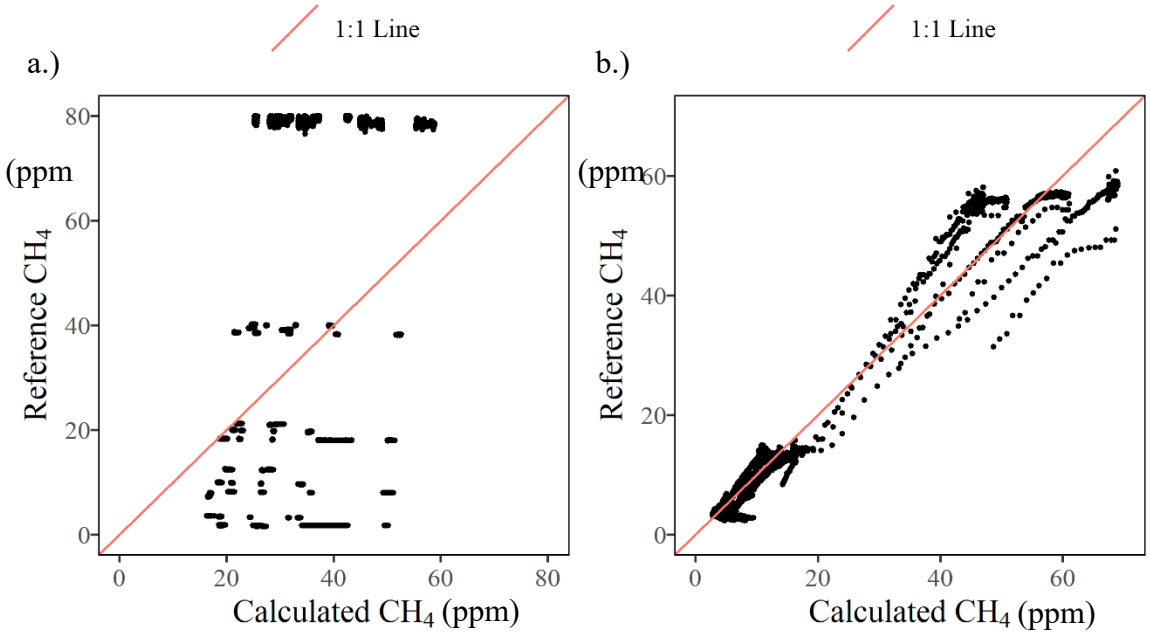


Figure 18 Comparison of reference $CH_4$ concentrations and calibrated low-cost sensor $CH_4$ concentrations during lab tests with variable (a) and stable (b) environments, similar to field conditions. In the absence of field data, these laboratory tests demonstrate the expected improvement by stabilizing the measurement environment.

### 3.4 Industrial Applications Evaluation

The final consideration in this research is to evaluate the sensor in the proposed application for industrial $CH_4$ emissions monitoring. An application that was explored for the MOS sensor was continuous site monitoring for oil and gas facilities. Prior to conducting any fieldwork, it was assumed that $CH_4$ emissions at these sites would be persistent sources lasting on the timescale of hours to weeks once they began emitting. This assumption was proven to be false at this compression station. There were large releases that occurred on a short timescale, often less than 5-10 seconds (Figure 16). Any persistent sources at this site were shadowed by the large magnitude of the intermittent sources. Additionally, as previously mentioned, the wind affected how the releases were measured. The instrument was installed down-wind of the sources, but with the natural

variability of the wind direction, the observed releases at the sensor were likely further shortened.

At the industrial field site, the pulse measurement by the reference instrument and by the MOS sensor were compared. Due to the previously described volume challenges, the sensor box was not used at this site, but a sensor without environmental controls was employed. The effects of humidity were evident as shown in the time series below (Figure 19).

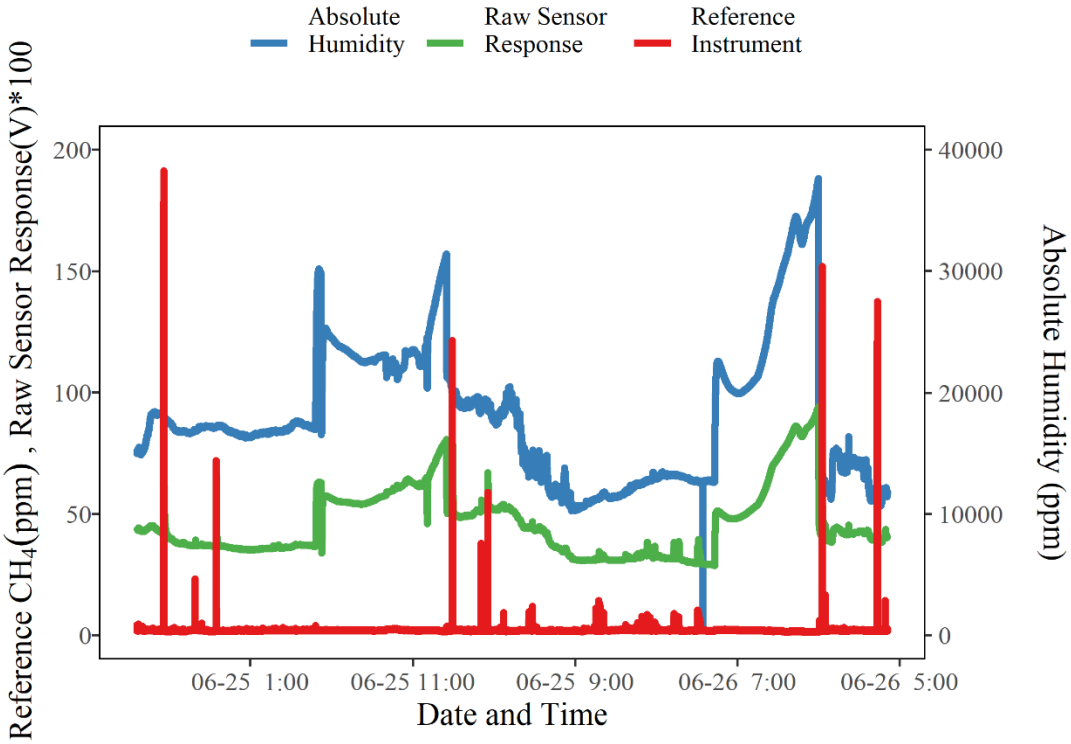


Figure 19 $CH_4$ concentration and humidity measured at an industrial site June 24-June 26, 2020. The raw sensor data (green) closely tracks the humidity data (blue).

Industrial $CH_4$ pulses have not been well characterized for the purposes of continuous ambient monitoring. The MOS sensor could detect the pulses, but the response was lagged, and the recovery after the pulse was longer than the reference instrument (Figure 20). Over two days, 21 significant pulses were measured, and the average length of those

pulses was 49 seconds (SD of 32) for the reference instrument, while on the MOS sensor the average length was 118 seconds. These pulses were not symmetrical, particularly those measured with the MOS sensor. There was both a lag and a smeared response compared to the reference instrument's measurements. Consecutive pulses over a short time also affected the MOS sensor response. When multiple pulses were measured by the reference instrument, the MOS sensor could not differentiate between separate pulses. The smearing of the MOS pulse means that the magnitude of any subsequent releases would not be reported consistently by the sensor (Figure 20b). The lag between instruments was likely partially due to the travel time between instruments as they were installed in series.

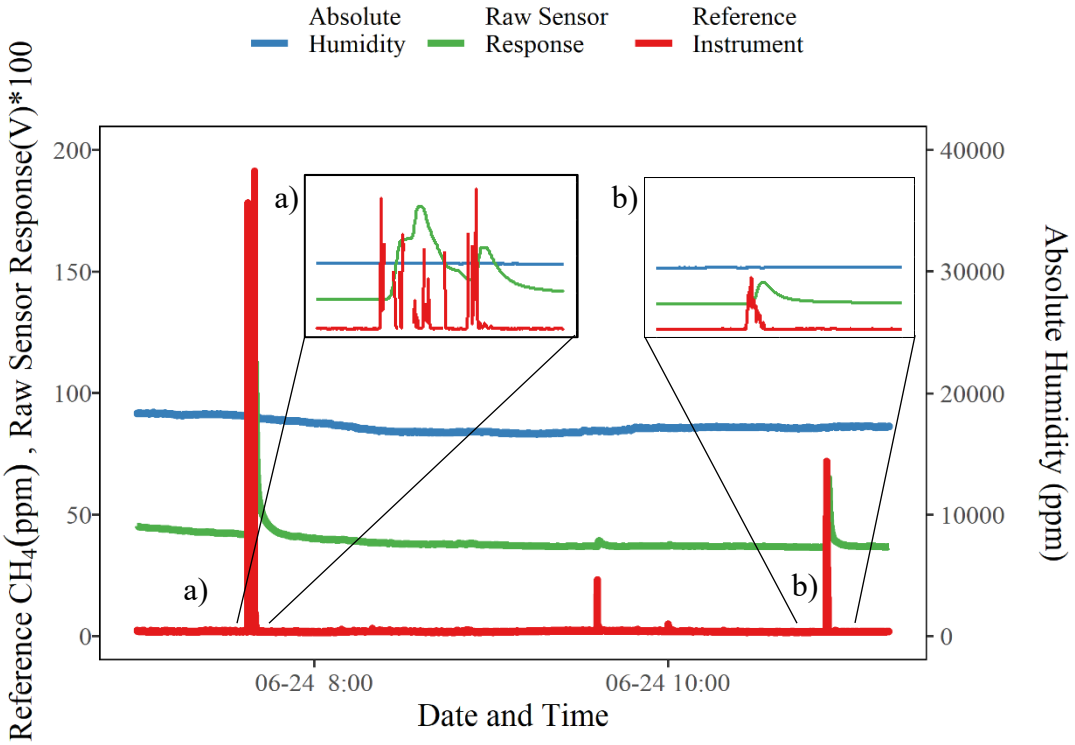


Figure 20 Two pulses recorded during a period with a stable humidity to demonstrate the difference between the pulses as measured with the reference instrument and those measured with the MOS sensor. Panel a) shows a sustained release, and b) shows a single pulse event.

Attempts were made to calibrate the sensor using lab calibration data, field derived calibration data, using the area under the curve of each pulse, and using a humidity correction. None of these methods were successful in predicting a $CH_4$ concentration of the pulse due to the changing resolution of the sensor before and after each pulse. While quantifying the sensor's response was not successful for this application, the sensor was able to detect all the large pulse events. The sensor was able to detect the occurrence of a methane release pulse, but without an accurate calibration the magnitude of the release could not be estimated.

# CHAPTER 4 DISCUSSION

The goal of this research was to evaluate a low-cost sensor and its performance in a stable measurement environment for use in environmental monitoring and more generally to advance knowledge in the use of these low-cost methane sensors. This research took a concept used elsewhere in sensing technologies (the use of a controlled measurement environment) (Crosson, 2008) and applied it to a new sensor type. The results demonstrated the limitations of the controlled environment and highlighted the challenges of working with MOS sensors on a large scale. Several important application-based considerations were revealed and can be built upon in future research.

## 4.1 Laboratory testing

The tests described in section 3.1 were designed based on a limited understanding of sensor needs at the time. Based on recent studies (Bastviken et al., 2020; Chan et al., 2020) about sensor requirements, this test set-up was not adequate to evaluate the sensor for ambient environmental monitoring. When evaluating the MOS sensor, testing should be conducted over a smaller range of temperatures and humidity levels that better reflect conditions in the field. Planning for the expected field conditions could decrease the range of temperatures over which calibration would be needed. In this research, temperatures above 50°C are not likely in a field application and would not be needed for future experiments with this sensor for outdoor monitoring. More importantly, to observe changes in atmospheric levels of $CH_4$, additional steps to better determine the sensor's ability to resolve small changes in $CH_4$ concentration would have been more helpful for future work. The evaluation tests in section 3.1 demonstrate significantly better performance than the specific manufacturer sheet implied, but also highlighted the

challenges related to working with the sensor and its sensitivities to changes in temperature and humidity. The study findings on the sensor's sensivity to environmental conditions are in general agreement with previous studies (Bastviken et al., 2020; Casey et al., 2019; Collier-Oxandale et al., 2018; Eugster & Kling, 2012; Van Den Bossche et al., 2017).

The MOS sensor showed considerably better performance than the manufacturer's specifications, as was also reported by (Bastviken et al., 2020; Casey et al., 2019; Collier-Oxandale et al., 2018; Eugster & Kling, 2012; Van Den Bossche et al., 2017). The initial laboratory testing also showed that there was less noise and better resolution between concentration steps at lower humidity levels than at the higher levels as shown in Figure 13. This humidity effect was unexpected and influenced the design of the sensor box with a focus on decreasing humidity in the box for improved resolution (Bastviken et al., 2020; Collier-Oxandale et al., 2018; Eugster & Kling, 2012; Van Den Bossche et al., 2017).While realtive humidity can be measured more readily, using absolute humidity in calibration equations improves the estimate, when using a calibration function (Bastviken et al., 2020).

### 4.2 Laboratory and Field Testing of Environmentally Controlled Enclosure

The traditional calibration method for these MOS sensors has been to take a reference instrument in the field and run both the reference instrument and MOS sensor in the field for a period and generate a field-specific calibration formula (Collier-Oxandale et al., 2018; Eugster et al., 2020). The ability to calibrate the instrument in the lab before going to the field is helpful for a remote site where there may not be ample power for reference instruments. A prime example of this would be in permafrost settings where operations

would be remote, but where methane release can be important (Christensen et al., 2004; Eugster et al., 2020). If the sensor box was calibrated in the lab under the expected field conditions, it could be taken into the field without the need for a reference instrument in the field. Additionally, with a low humidity and stable temperature the calibration process is simplified as corrections for temperature and humidity are no longer needed in the field.

Based on the laboratory results, an RMSE of between 2 and 5 ppm for the sensor box would be expected. These results are significantly better than the manufacturer's specifications and demonstrate that the sensor's minimum detection limit is substantially lower than 500 ppm, the manufacturer's specified lower range. Since Eugster and Kling's early methane MOS sensor research in 2012, a great deal has been learned about how best to use these sensors. Eugster and Kling first suggested using MOS sensors in atmospheric applications and reported a detection limit lower than 500 ppm, but had challenges with sensor interferences. Additional research has continued to improve detection limits suggesting, based largely on laboratory studies, that the MOS sensors have potential as atmospheric monitoring tools (Van Den Bossche et al., 2017) and report sub-ppm resolution in a laboratory environment. More recent field research (Bastviken et al., 2020) reported RMSE values from different calibration methods which are in line with this research (2.5 - 36 ppm).

These results also show the potential of the sensor box in improving the sensor performance. The expected error with the sensor box is nearly 10 times lower than the expected error with no environmental controls.

$CH_4$ concentration data, along with supporting measurements, can be used to estimate an emissions rate from a source. Emissions plume modeling would require measurements with an error less than 1 ppm. For industrial monitoring, knowing the $CH_4$ release rate is important for regulatory compliance. Controlling the measurement environment has been successful for other applications (Crosson, 2008), but the expected error in the low ppm range (< 5 ppm) would be better suited for $CH_4$ source detection than for quantification of $CH_4$ emissions. The sensor was able to detect large releases in the field study, suggesting that an ideal application for this sensor would be as a continuous monitoring screening tool for $CH_4$ leaks or other pulse events similar to a household smoke alarm. The sensor could indicate if a release occurs, and a more accurate instrument could be used to quantify the release.

The accuracy of ~1 ppm under stable temperature and low humidity (Table 5) represents the best achievable performance in the sensor box. It is below ambient $CH_4$ concentration levels and would be suitable for many applications, particularly industrial leak detection for which $CH_4$ concentration peaks in recent field testing in this research and in that completed by others ranged from 3 ppm to more than 300 ppm (Golston et al., 2018). However, it would not be suitable for estimating emissions rates (or flux) from atmospheric measurement where ppb-level resolution is required for inversion modelling (Edie et al., 2020; U.S. EPA, 2014).

The testing results of this study show that the determined MOS sensor resolution is similar to other recent research, such as Bastviken et al. (2020), where the same sensor was evaluated under similar environmental conditions as described in sections 3.2 and 3.3. Other MOS research resulted in improved RMSE but focused on a smaller range of

$CH_4$ concentrations (<10 ppm) (Casey et al., 2019; Collier-Oxandale et al., 2018; Eugster & Kling, 2012; Van Den Bossche et al., 2017). Carefully considering the application and end-use of the data will make the sensor most useful.

### 4.3 Industrial Applications Evaluation

An important finding of this research is that considering the timescale on which changes in concentration happen is important to determine the MOS sensor suitability. The changes that occurred during laboratory calibrations were all conducted over time periods of greater than 10 minutes, while in the field changes occurred in seconds. These quick pulse responses were not studied in the laboratory prior to the field work, nor did previous studies include pulse events on the same magnitude as those observed at the industrial field site (Bastviken et al., 2020; Collier-Oxandale et al., 2018). The MOS sensor response time was lagged, and the return to baseline was smeared compared to the reference analyzer (Figure 20). This meant that determining the magnitude of the concentration pulse and the detection of subsequent $CH_4$ peaks was not possible. The sensor, as it was set up, could underestimate the quantity and magnitude of release events. The volume of the measurement enclosure, in particular, was a significant challenge to using the MOS sensor in the field. The sensor was housed in an enclosure with a relatively large volume (approximately 2 L). The pulses occurred on a short timescale which meant that the gas was diluted upon entering the measurement enclosure. The dilution combined with the sensor's response time resulted in none of the methane peaks that were detected by the reference instrument being detected by the MOS sensor.

Using a small enclosure around the sensor alone would improve the sensor's usability for a field application. The large enclosure contained several other sensors along with baffles

to mix the gas in the enclosure, but this design does not work for measurements that change on the timescale of seconds. Using a larger volume enclosure would be more suitable for monitoring changes that happen over days where there is the opportunity for the gas to fill the enclosure with a representative sample. At industrial sites, this could include near source monitoring, where wind wouldn't cause the appearance of pulse events or monitoring soil gas migration from underground infrastructure. For ambient industrial monitoring, as was done in this study, individual sensors could be installed in series with much smaller individual sensor enclosures, which would reduce the volume by several orders of magnitude. If using several sensors, the MOS sensor could be installed at the first sensor in the series to further reduce dilution effects.

Additionally, the MOS sensor's response time imposed limits on the pulse detection. The response time and nature of the emissions made calibration of the sensor in the field unfeasible. The MOS response time was slower than the reference instrument. A time lag alone can be managed during data processing. The difference in response speed between the MOS sensor and reference instrument could also be processed by calibrating based on the peaks in the responses. The difficulty in calibrating was observed when there were several pulse events in short succession. As described above, pulses measured by the MOS sensor shortly after a large pulse would not peak in the same way as they would have had they been measured after a period of time with no releases. This is an important challenge for an MOS sensor in an industrial monitoring environment. The MOS sensor's operating principle relies on fresh air to replenish the oxygen on the sensing layer (Wang et al., 2010). A possible explanation for the slow return to baseline and the decreased sensitivity after a large pulse is that oxygen layer had not yet been replenished and the

sensor was not operating at peak resolution during these times. This phenomenon will require additional research to develop hardware or analytical-based solutions. It would not impact the sensor's use as a leak detector but does create additional challenges for accurately estimating emissions rates.

### 4.4 Additional Considerations

An important reason for finding low-cost $CH_4$ measurement tools is to improve $CH_4$ inventories and reduce their uncertainties. Low-cost sensors offer a great deal of potential for large scale grid monitoring, but this research highlights several considerations in the usability of the sensor for industrial monitoring. Many natural sources of $CH_4$ vary on longer timescales and over smaller ranges (with a notable exception being ebullition in wetlands) than the industrial emissions observed in this research (Vaughn et al., 2018). In addition to challenges imposed from different emission sources, measuring methane concentrations down wind of a source will also make a source behave like an intermittent source with many short pulses as the wind changes directions. To capture these short pulse events, a pump with a high flow rate will increase the volume of gas sampled and increase the likelihood of measuring a short-lived emission event. This approach should be paired with taking high frequency measurements (at least 1 Hz) and minimizing the measurement volume as previously described.

This project's scope initially included additional low-cost sensors. The project scope was narrowed to focus on the environmental enclosure; however, the use of other low-cost sensors would be worth examining. Studying the behavior between sensors and using ratios between different gas measurements could improve the sensor's usability. The

ratios could be used to improve baseline measurements, to identify different sources, and to perhaps better characterize the gas being measured.

# CHAPTER 5 CONCLUSIONS

With increasing pressure to quantify climate change risks and to understand $CH_4$ emission sources by governments around the world, there is an increasing demand for low-cost $CH_4$ monitoring tools. MOS sensors have been proposed as a solution for industries such as oil and gas to meet increasing regulatory pressures. The MOS sensor has the potential for use in industrial monitoring. Its low-cost and low-power requirements make it a strong candidate for use in larger monitoring networks. MOS sensors often have strong selectivity for $CH_4$ and can detect $CH_4$ at ppm levels.

However, these sensors do also have many challenges for wide-scale deployment. The humidity sensitivity and sensor response time create significant challenges for measuring ambient environmental $CH_4$ changes. Humidity has a very strong influence on the sensor response and will need to be considered in future MOS sensor research. Future work with the MOS sensor should concentrate on either improved humidity regulation or correction. The sensor box demonstrated potential, and work to improve it should include reducing the volume inside of the gas sensor enclosure to reduce dilution when measuring. While stabilizing environmental conditions did improve the sensor's performance, the improvement was not sufficient to make the sensor a suitable tool to estimate gas emissions rates. For this purpose, improved accuracy is required.

Future work exploring the use of MOS sensors for industrial monitoring should bring sensor response time into consideration when designing $CH_4$ monitoring tools for industrial applications. In considering the sensor's slow response, the sensor is likely

better suited to monitoring applications where the concentration changes happen over a longer time scales, as opposed to pulse events.

MOS sensors continue to offer potential as low-cost sensing solutions. These results highlight the challenges of working with MOS sensors in industrial environments. Using an MOS sensor requires careful consideration of the application and the sensor environment. Continued research to support further development of MOS sensors for environmental gas monitoring can improve the accuracy of the global methane budget by developing a large monitoring network and thereby support efforts to understand and mitigate climate change.

## REFERENCES


Aldhafeeri, T., Tran, M. K., Vrolyk, R., Pope, M., & Fowler, M. (2020). A review of methane gas detection sensors: Recent developments and future perspectives. *Inventions*, *5*(3), 1–18. https://doi.org/10.3390/inventions5030028

Allen, G. (2016). Rebalancing the global methane budget. *Nature*, *538*(7623), 46. https://doi.org/10.1038/538046a

Bastviken, D, Nygren, J., Schenk, J., Parellada Massana, R., & Duc, N. T. (2020). Technical note: Facilitating the use of low-cost methane (\chem{CH_{4}}) sensors in flux chambers -- calibration, data processing, and an open-source make-it-yourself logger. *Biogeosciences*, *17*(13), 3659–3667. https://doi.org/10.5194/bg-17-3659-2020

Bastviken, David, Nygren, J., Schenk, J., Parellada Massana, R., & Thanh Duc, N. (2020). Technical note: Facilitating the use of low-cost methane (ch4) sensors in flux chambers-calibration, data processing, and an open-source make-it-yourself logger. *Biogeosciences*, *17*(13), 3659–3667. https://doi.org/10.5194/BG-17-3659-2020

Berge, A., & Johansson, P. (2012). *Literature Review of High Performance Thermal Insulation Report in Building Physics*. http://publications.lib.chalmers.se/records/fulltext/local_159807.pdf

Besson, J.-P., Schilt, S., & Thévenaz, L. (2006). Sub-ppm multi-gas photoacoustic sensor. *Spectrochimica Acta Part A*, *63*, 899–904.

https://doi.org/10.1016/j.saa.2005.10.034

Brown, A., Hayward, T., Timmis, R., Wade, K., Pope, R., Trent, T., Boesch, H., & Guillo, R. B. (2021). *Satellite measurements of air quality and greenhouse gases: application to regulatory activities* (Issue May). www.gov.uk/environment-agency

Casey, J. G., Collier-Oxandale, A., & Hannigan, M. (2019). Performance of artificial neural networks and linear models to quantify 4 trace gas species in an oil and gas production region with low-cost sensors. *Sensors and Actuators B: Chemical*, *283*, 504–514. https://doi.org/10.1016/j.snb.2018.12.049

Chan, E., Worthy, D. E. J., Chan, D., Ishizawa, M., Moran, M. D., Delcloo, A., & Vogel, F. (2020). Eight-Year Estimates of Methane Emissions from Oil and Gas Operations in Western Canada Are Nearly Twice Those Reported in Inventories. *Environmental Science and Technology*, *54*(23), 14899–14909. https://doi.org/10.1021/acs.est.0c04117

Christensen, T. R., Johansson, T., Åkerman, H. J., Mastepanov, M., Malmer, N., Friborg, T., Crill, P., & Svensson, B. H. (2004). Thawing sub-arctic permafrost: Effects on vegetation and methane emissions. *Geophysical Research Letters*, *31*(4). https://doi.org/https://doi.org/10.1029/2003GL018680

Collier-Oxandale, A., Casey, J. G., Piedrahita, R., Ortega, J., Halliday, H., Johnston, J., & Hannigan, M. P. (2018). Assessing a low-cost methane sensor quantification system for use in complex rural and urban environments. *Atmos. Meas. Tech*, *11*, 3569–3594. https://doi.org/10.5194/amt-11-3569-2018

Crosson, E. R. (2008). A cavity ring-down analyzer for measuring atmospheric levels of methane, carbon dioxide, and water vapor. *Applied Physics B: Lasers and Optics*, *92*(3 SPECIAL ISSUE), 403–408. https://doi.org/10.1007/s00340-008-3135-y

Dinh, T.-V., Choi, I.-Y., Son, Y.-S., & Kim, J.-C. (2016). A review on non-dispersive infrared gas sensors: Improvement of sensor detection limit and interference correction. *Sensors and Actuators B: Chemical*, *231*, 529–538. https://doi.org/10.1016/J.SNB.2016.03.040

Dlugokencky, E. (2020). *No Title*. NOAA/GML. https://gml.noaa.gov/ccgg/trends_ch4/

Dlugokencky, E. J. (2018). *Trends in Atmospheric Methane*. NOAA/ESRL. https://www.esrl.noaa.gov/gmd/ccgg/trends_ch4/

Dlugokencky, E. J., Nisbet, E. G., Fisher, R., & Lowry, D. (2011). Global atmospheric methane: Budget, changes and dangers. *Philosophical Transactions of the Royal Society A: Mathematical, Physical and Engineering Sciences*, *369*(1943), 2058–2072. https://doi.org/10.1098/rsta.2010.0341

Dlugokencky, E. J., Steele, L. P., Lang, P. M., & Masarie, K. A. (1995). Atmospheric methane at Mauna Loa and Barrow observatories: Presentation and analysis of in situ measurements. *Journal of Geophysical Research*, *100*(D11), 23103. https://doi.org/10.1029/95JD02460

Edie, R., Robertson, A. M., Field, R. A., Soltis, J., Snare, D. A., Zimmerle, D., Bell, C. S., Vaughn, T. L., & Murphy, S. M. (2020). Constraining the accuracy of flux estimates using OTM 33A. *Atmos. Meas. Tech.*, *13*(1), 341–353.

https://doi.org/10.5194/amt-13-341-2020

Ehret, G., Bousquet, P., Pierangelo, C., Alpers, M., Millet, B., Abshire, J., Bovensmann, H., Burrows, J., Chevallier, F., Ciais, P., Crevoisier, C., Fix, A., Flamant, P., Frankenberg, C., Gibert, F., Heim, B., Heimann, M., Houweling, S., Hubberten, H., … Wirth, M. (2017). MERLIN: A French-German Space Lidar Mission Dedicated to Atmospheric Methane. *Remote Sensing*, *9*(10), 1052. https://doi.org/10.3390/rs9101052

Elkind, J., Blanton, E., Denier van der Gon, H., Leemhuis, A., & Kleinberg, R. (2020). Nowhere to Hide: Implications for Policy, Industry, and Finance of Satellite-Based Methane Detection. *Columbia SIPA*, *October*, 1–19. https://www.energypolicy.columbia.edu/research/commentary/nowhere-hide-implications-policy-industry-and-finance-satellite-based-methane-detection

Environment and Climate Change Canada. (2020). *Sources and Sinks in Canada Canada's Submission To the United Nations Framework*.

Environment Canada. (2018). *Canadian Climate Normals Halifax Stanfield Airport Station Data 1981-2010*. http://climate.weather.gc.ca/climate_normals/results_1981_2010_e.html?searchType=stnProv&lstProvince=NS&txtCentralLatMin=0&txtCentralLatSec=0&txtCentralLongMin=0&txtCentralLongSec=0&stnID=6358&dispBack=0

Eugster, W, & Kling, G. W. (2012). Performance of a low-cost methane sensor for ambient concentration measurements in preliminary studies. *Atmospheric*

*Measurement Techniques*, *5*(8), 1925–1934. https://doi.org/10.5194/amt-5-1925-2012

Eugster, Werner, Laundre, J., Eugster, J., & Kling, G. W. (2020). Long-term reliability of the Figaro TGS 2600 solid-state methane sensor under low-Arctic conditions at Toolik Lake, Alaska. *Atmospheric Measurement Techniques*, *13*(5), 2681–2695. https://doi.org/10.5194/amt-13-2681-2020

Figaro Inc. (2012). *Application Notes for Methane Gas Detectors using TGS2611*.

Filipovic, L., & Selberherr, S. (2015). Performance and stress analysis of metal oxide films for CMOS-integrated gas sensors. *Sensors (Switzerland)*, *15*(4), 7206–7227. https://doi.org/10.3390/s150407206

Forster, P. M., Storelvmo, T., Armour, K., Collins, W., Dufresne, J. L., Frame, D., Lunt, D. J., Mauritsen, T., Palmer, M. D., Watanabe, M., Wild, M., & Zhang, H. (2021). Chapter 7: The Earth's Energy Budget, Climate Feedbacks, and Climate Sensitivity. In *Climate Change 2021: The Physical Science Basis. Contribution of Working Group I to the Sixth Assessment Report of the Intergovernmental Panel on Climate Change* (Issue August).

Gallucci, M. (2020). *New Microsatellite Will Focus on Industrial Methane Emissions - IEEE Spectrum*. IEEE Spectrum. https://spectrum.ieee.org/microsatellite-industrial-methane-emissions

Golston, L., Aubut, N., Frish, M., Yang, S., Talbot, R., Gretencord, C., McSpiritt, J., & Zondlo, M. (2018). Natural Gas Fugitive Leak Detection Using an Unmanned Aerial

Vehicle: Localization and Quantification of Emission Rate. *Atmosphere*, *9*(9), 333. https://doi.org/10.3390/atmos9090333

Ito, A., & Inatomi, M. (2012). Use of a process-based model for assessing the methane budgets of global terrestrial ecosystems and evaluation of uncertainty. *Biogeosciences*, *9*(2), 759–773. https://doi.org/10.5194/bg-9-759-2012

Jackson, R. B., Saunois, M., Bousquet, P., Canadell, J. G., Poulter, B., Stavert, A. R., Bergamaschi, P., Niwa, Y., Segers, A., & Tsuruta, A. (2020). *Increasing anthropogenic methane emissions arise equally from agricultural and fossil fuel sources*. *15*(7), 71002. https://doi.org/10.1088/1748-9326/ab9ed2

Jacob, D. J., Turner, A. J., Maasakkers, J. D., Sheng, J., Sun, K., Liu, X., Chance, K., Aben, I., McKeever, J., & Frankenberg, C. (2016). Satellite observations of atmospheric methane and their value for quantifying methane emissions. *Atmos. Chem. Phys*, *16*, 14371–14396. https://doi.org/10.5194/acp-16-14371-2016

Joos, F., Roth, R., Fuglestvedt, J. S., Peters, G. P., Enting, I. G., Von Bloh, W., Brovkin, V., Burke, E. J., Eby, M., Edwards, N. R., Friedrich, T., Frölicher 11, T. L., Halloran, P. R., Holden, P. B., Jones, C., Kleinen, T., Mackenzie, F. T., Matsumoto, K., Meinshausen, M., … Weaver, A. J. (2013). Carbon dioxide and climate impulse response functions for the computation of greenhouse gas metrics: a multi-model analysis. *Atmospheric Chemistry and Physics*, *13*, 2793–2825. https://doi.org/10.5194/acp-13-2793-2013

Kirschke, S., Bousquet, P., Ciais, P., Saunois, M., Canadell, J. G., Dlugokencky, E. J.,

Bergamaschi, P., Bergmann, D., Blake, D. R., Bruhwiler, L., Cameron-Smith, P., Castaldi, S., Chevallier, F., Feng, L., Fraser, A., Heimann, M., Hodson, E. L., Houweling, S., Josse, B., … Zeng, G. (2013). Three decades of global methane sources and sinks. *Nature Geoscience*, *6*(10), 813–823. https://doi.org/10.1038/ngeo1955

Knox, S. H., Jackson, R. B., Poulter, B., McNicol, G., Fluet-Chouinard, E., Zhang, Z., Hugelius, G., Bousquet, P., Canadell, J. G., Saunois, M., Papale, D., Chu, H., Keenan, T. F., Baldocchi, D., Torn, M. S., Mammarella, I., Trotta, C., Aurela, M., Bohrer, G., … Zona, D. (2019). FLUXNET-CH4 Synthesis Activity: Objectives, Observations, and Future Directions. *Bulletin of the American Meteorological Society*, *100*(12), 2607–2632. https://doi.org/10.1175/BAMS-D-18-0268.1

Lan, X., Nisbet, E. G., Dlugokencky, E. J., & Michel, S. E. (2021). What do we know about the global methane budget? Results from four decades of atmospheric CH 4 observations and the way forward . *Philosophical Transactions of the Royal Society A: Mathematical, Physical and Engineering Sciences*, *379*(2210), 20200440. https://doi.org/10.1098/rsta.2020.0440

Lawrence, N. S. (2006). Analytical detection methodologies for methane and related hydrocarbons. *Talanta*, *69*(2), 385–392. https://ac-els-cdn-com.ezproxy.library.dal.ca/S0039914005006739/1-s2.0-S0039914005006739-main.pdf?_tid=f91ef538-7086-4d81-93ad-0c6700ab878e&acdnat=1540151198_c4350db2515b7f08a178e27b5692bf80

Liu, F., Zhang, Y., Yu, Y., Xu, J., Sun, J., & Lu, G. (2011). Enhanced sensing

performance of catalytic combustion methane sensor by using Pd nanorod/-Al 2 O 3. *Sensors and Actuators B*, *160*, 1091–1097. https://doi.org/10.1016/j.snb.2011.09.032

Lyon, D. R., Alvarez, R. A., Zavala-Araiza, D., Brandt, A. R., Jackson, R. B., & Hamburg, S. P. (2016). Aerial Surveys of Elevated Hydrocarbon Emissions from Oil and Gas Production Sites. *Environmental Science and Technology*, *50*(9), 4877–4886. https://doi.org/10.1021/acs.est.6b00705

Masson, N., Piedrahita, R., & Hannigan, M. (2015). Approach for quantification of metal oxide type semiconductor gas sensors used for ambient air quality monitoring. *Sensors & Actuators: B. Chemical*, *208*, 339–345. https://doi.org/10.1016/j.snb.2014.11.032

Myhre, G., Shindell, D., Breon, F.-M., Collins, W., Fuglestvedt, J., Huang, J., Koch, D., Lamarque, J.-F., Lee, D., Mendoza, B., Nakajima, T., Robock, A., Stephens, G., Takemura, T., & Zhang, H. (2013). Anthropogenic and natural radiative forcing. In T. F. Stocker, D. Qin, G.-K. Plattner, M. Tignor, S. K. Allen, J. Boschung, A. Nauels, Y. Xia, V. Bex, & P. M. Midgley (Eds.), *Climate Change 2013 the Physical Science Basis: Working Group I Contribution to the Fifth Assessment Report of the Intergovernmental Panel on Climate Change* (pp. 659–740). Cambridge University Press. https://doi.org/10.1017/CBO9781107415324.018

Nagai, D., Nishibori, M., Itoh, T., Kawabe, T., Sato, K., & Shin, W. (2015). Ppm level methane detection using micro-thermoelectric gas sensors with Pd/Al2O3combustion catalyst films. *Sensors and Actuators, B: Chemical*, *206*, 488–494. https://doi.org/10.1016/j.snb.2014.09.059

National Academies of Sciences Engineering and Medicine. (2018). *Improving Characterization of Anthropogenic Methane Emissions in the United States*. The National Academies Press. https://doi.org/10.17226/24987

Nisbet, E. G., Fisher, R. E., Lowry, D., France, J. L., Allen, G., Bakkaloglu, S., Broderick, T. J., Cain, M., Coleman, M., Fernandez, J., Forster, G., Griffiths, P. T., Iverach, C. P., Kelly, B. F. J., Manning, M. R., Nisbet-Jones, P. B. R., Pyle, J. A., Townsend-Small, A., al-Shalaan, A., … Zazzeri, G. (2020). Methane Mitigation: Methods to Reduce Emissions, on the Path to the Paris Agreement. *Reviews of Geophysics*, *58*(1), e2019RG000675. https://doi.org/https://doi.org/10.1029/2019RG000675

Pearce, T. C., Schiffman, S. S., Nagle, H. T., & Gardner, J. W. (Eds.). (2003). *Handbook of Machine Olfaction*. Wiley - VCH. https://doi.org/10.1002/3527601597

Peischl, J., Karion, A., Sweeney, C., Kort, E. A., Smith, M. L., Brandt, A. R., Yeskoo, T., Aikin, K. C., Conley, S. A., Gvakharia, A., Trainer, M., Wolter, S., & Ryerson, T. B. (2016). Quantifying atmospheric methane emissions from oil and natural gas production in the Bakken shale region of North Dakota. *Journal of Geophysical Research: Atmospheres*, *121*(10), 6101–6111. https://doi.org/https://doi.org/10.1002/2015JD024631

Perma Pure LLC. (n.d.). *Perma Pure Purge Gas Configurations*. Retrieved February 10, 2017, from https://www.permapure.com/products/gas-sample-dryers/perma-pure-purge-gas-configurations/

Peterson, P. J. D. D., Aujla, A., Grant, K. H., Brundle, A. G., Thompson, M. R., Vande Hey, J., Leigh, R. J., Peterson, P. J. D. D., Aujla, A., Grant, K. H., Brundle, A. G., Thompson, M. R., Vande Hey, J., Leigh, R. J., Hey, J. Vande, & Leigh, R. J. (2017). Practical Use of Metal Oxide Semiconductor Gas Sensors for Measuring Nitrogen Dioxide and Ozone in Urban Environments. *Sensors*, *17*(7), 1653. https://doi.org/10.3390/s17071653

Qi, Q., Zhang, T., Zheng, X., Fan, H., Liu, L., Wang, R., & Zeng, Y. (2008). Electrical response of Sm 2 O 3-doped SnO 2 to C 2 H 2 and effect of humidity interference. *Sensors and Actuators B*, *134*, 36–42. https://doi.org/10.1016/j.snb.2008.04.011

R Core Team. (2020). *R: A Language and Environment for Statistical Computing*. R Foundation for Statistical Computing. https://www.r-project.org/

Rouxel, J., Coutard, J.-G. G., Gidon, S., Lartigue, O., Nicoletti, S., Parvitte, B., Vallon, R., Zéninari, V., & Glière, A. (2015). Development of a miniaturized differential photoacoustic gas sensor. *Procedia Engineering*, *120*, 396–399. https://doi.org/10.1016/j.proeng.2015.08.650

Saunois, M., Bousquet, P., Poulter, B., Peregon, A., Ciais, P., Canadell, J. G., Dlugokencky, E. J., Etiope, G., Bastviken, D., Houweling, S., Janssens-Maenhout, G., Tubiello, F. N., Castaldi, S., Jackson, R. B., Alexe, M., Arora, V. K., Beerling, D. J., Bergamaschi, P., Blake, D. R., … Zhu, Q. (2016). The global methane budget 2000-2012. *Earth System Science Data*, *8*(2), 697–751. https://doi.org/10.5194/essd-8-697-2016

Saunois, M., Stavert, A. R., Poulter, B., Bousquet, P., Canadell, J. G., Jackson, R. B., Raymond, P. A., Dlugokencky, E. J., & Houweling, S. (2020). *The Global Methane Budget 2000 – 2017*. 1561–1623.

Sohn, J. H., Atzeni, M., Zeller, L., & Pioggia, G. (2008). Characterisation of humidity dependence of a metal oxide semiconductor sensor array using partial least squares. *Sensors and Actuators B*, *131*, 230–235. https://doi.org/10.1016/j.snb.2007.11.009

Spinelle, L., Gerboles, M., Villani, M. G., Aleixandre, M., & Bonavitacola, F. (2015). Field calibration of a cluster of low-cost available sensors for air quality monitoring. Part A: Ozone and nitrogen dioxide. *Sensors and Actuators B*, *215*, 249–257. https://doi.org/10.1016/j.snb.2015.03.031

Sun, P., Jiang, Y., Xie, G., Du, X., & Hu, J. (2009). A room temperature supramolecular-based quartz crystal microbalance (QCM) methane gas sensor. *Sensors and Actuators, B: Chemical*, *141*(1), 104–108. https://doi.org/10.1016/j.snb.2009.06.012

Tans, P., & Keeling, R. (2018). *Trends in Atmospheric Carbon Dioxide*. NOAA/ESRL.

Thompson, R. L., Stohl, A., Zhou, L. X., Dlugokencky, E., Fukuyama, Y., Tohjima, Y., Kim, S.-Y., Lee, H., Nisbet, E. G., Fisher, R. E., Lowry, D., Weiss, R. F., Prinn, R. G., O'Doherty, S., Young, D., & White, J. W. C. (2015). Methane emissions in East Asia for 2000–2011 estimated using an atmospheric Bayesian inversion. *Journal of Geophysical Research: Atmospheres*, *120*(9), 4352–4369. https://doi.org/https://doi.org/10.1002/2014JD022394

U.S. EPA. (2014). *Other Test Method (OTM) 33 and 33A Geospatial Measurement of Air*

*Pollution-Remote Emissions Quantification-Direct Assessment (GMAP-REQ-DA)*.

Van Den Bossche, M., Rose, N. T., Franz, S., & De Wekker, J. (2017). Potential of a low-cost gas sensor for atmospheric methane monitoring. *Sensors & Actuators: B. Chemical*, *238*, 501–509. https://doi.org/10.1016/j.snb.2016.07.092

Vaughn, T. L., Bell, C. S., Pickering, C. K., Schwietzke, S., Heath, G. A., Pétron, G., Zimmerle, D. J., Schnell, R. C., & Nummedal, D. (2018). Temporal variability largely explains top-down/bottom-up difference in methane emission estimates from a natural gas production region. *Proceedings of the National Academy of Sciences*, *115*(46), 11712–11717. https://doi.org/10.1073/PNAS.1805687115

Wang, C., Yin, L., Zhang, L., Xiang, D., & Gao, R. (2010). Metal oxide gas sensors: sensitivity and influencing factors. *Sensors (Basel, Switzerland)*, *10*(3), 2088–2106. https://doi.org/10.3390/s100302088

Wen, G., Zheng, J., Zhao, C., Shuang, S., Dong, C., & Choi, M. M. F. F. (2008). A microbial biosensing system for monitoring methane. *Enzyme and Microbial Technology*, *43*(3), 257–261. https://doi.org/10.1016/j.enzmictec.2008.04.006

World Meteorological Institute. (n.d.). *Observing Systems Capability Analysis and Review Tool - Space-based Capabilities*. Retrieved September 5, 2021, from https://space.oscar.wmo.int/gapanalyses?variable=23

Zellweger, C., Emmenegger, L., Firdaus, M., Hatakka, J., Heimann, M., Kozlova, E., Spain, T. G., Steinbacher, M., Van Der Schoot, M. V, & Buchmann, B. (2016). Assessment of recent advances in measurement techniques for atmospheric carbon

dioxide and methane observations. *Atmos. Meas. Tech*, *9*, 4737–4757. https://doi.org/10.5194/amt-9-4737-2016

Zhu, Z., Xu, Y., & Jiang, B. (2012). A one ppm NDIR methane gas sensor with single frequency filter denoising algorithm. *Sensors (Switzerland)*, *12*(9), 12729–12740. https://doi.org/10.3390/s120912729